



HAL
open science

On the low- and mid-frequency forced response of elastic structures using wave finite elements with one-dimensional propagation

Jean-Mathieu Mencik

► **To cite this version:**

Jean-Mathieu Mencik. On the low- and mid-frequency forced response of elastic structures using wave finite elements with one-dimensional propagation. *Computers & Structures*, 2010, 88, pp.674-689. 10.1016/j.compstruc.2010.02.006 . hal-00755757

HAL Id: hal-00755757

<https://hal.science/hal-00755757>

Submitted on 21 Nov 2012

HAL is a multi-disciplinary open access archive for the deposit and dissemination of scientific research documents, whether they are published or not. The documents may come from teaching and research institutions in France or abroad, or from public or private research centers.

L'archive ouverte pluridisciplinaire **HAL**, est destinée au dépôt et à la diffusion de documents scientifiques de niveau recherche, publiés ou non, émanant des établissements d'enseignement et de recherche français ou étrangers, des laboratoires publics ou privés.

On the low- and mid-frequency forced response of elastic structures using wave finite elements with one-dimensional propagation

J.-M. Mencik

*ENI Val de Loire, Université François Rabelais de Tours, LMR, Rue de la Chocolaterie, BP 3410,
F-41034 Blois Cedex, France*

Abstract

In this paper, the Wave Finite Element (WFE) method is investigated for computing the low- and mid-frequency forced response of straight elastic structures. The method uses wave modes as representation basis. These are numerically calculated using the finite element model of a typical substructure with a small number of degrees of freedom, and invoking Bloch's theorem. The resulting wave-based boundary value problem is presented and adapted so as to address Neumann-to-Dirichlet problems involving single as well as coupled structures. A regularization strategy is also presented. It improves the convergence of the WFE method when multi-layered systems are specifically dealt with. It employs an alternative form of the wave-based boundary value problem quite stable and easy to solve. The relevance of both classic and regularized WFE formalisms is discussed and numerically established compared with standard finite element solutions.

Key words: Wave propagation, finite elements, wave mode expansion, multi-layered systems, regularization.

Email address: jean-mathieu.mencik@univ-tours.fr (J.-M. Mencik)

1. Introduction

Slender straight elastic structures with uniform cross-sections are extensively encountered in many engineering areas, such as those involved in the manufacturing of chassis frames or aircraft fuselages. Such structures can reveal complex cross-sections as well as they can exhibit a relative complexity within the spatial distribution of their vibratory behavior, especially when the characteristic wavelengths reach the same order as the cross-section dimensions. This short wavelength domain is referred to as the mid-frequency range, where the cross-section reveals local resonances with a frequency distribution which can exhibit large variations [1]. This study concerns the use of the Wave Finite Element (WFE) method for predicting the low- and mid-frequency (LF and MF) vibratory behavior of such structures. In this framework, these are supposed to be constituted by a set of identical substructures connected along a main direction, perpendicular to the cross-section (see Figure 1). The WFE formalism uses numerical wave modes as expansion bases for describing the kinematic variables of these structures, that is the displacements and external/internal forces. The wave modes are numerically computed using the finite element (FE) model of a typical substructure [2, 3] (see Figure 1), whose mass and stiffness matrices can be simply obtained via commercial packages. The wave modes refer to as specific cross-section shapes traveling with specific velocities along the main direction of these slender systems. Parity among waves is well transcribed through the WFE modeling, in the sense that each positive-going wave mode is associated with a negative-going wave mode of the same velocity. Note that in the present work, positive- and negative-going waves will be denoted as incident and reflected modes (see Figure 1). The wave modes involve the standard propagating and evanescent wave motions — i.e. longitudinal, flexural, torsional and shearing — and additional MF solutions with non-uniform

cross-section shapes. In the WFE framework, the mesh density over the substructure cross-section can be adapted so as to address a sufficient number of highly oscillating wave shapes, depending on the frequency range considered. The two main features of the WFE method are that it is not constrained by LF analytical assumptions (e.g. the cross-section remains plane after deformation) and that it provides a large decrease of the CPU time for computing the forced responses of systems compared to the standard Finite Element Method [4]. This is explained as it involves relatively small numerical models whose dimensions reflect the cross-section dynamics only.

The WFE method has been widely used in the last few years for describing the one-dimensional wave propagation into systems of different natures (see for instance ref. [5] for beam-like structures, refs. [6, 7] for fluid-filled pipes, ref. [8] for laminates and ref. [9] for tyres). Also, it has been applied for predicting the forced response of elastic systems such as Euler-Bernoulli beams [10], simply supported Kirchhoff-Love plates [11, 10] and tyres [9]. The WFE strategy for computing the forced responses is not new (see for instance refs. [12, 13]) and requires an expansion of the kinematic variables onto wave mode bases with appropriate dimensions. The numerical issues associated with the resulting wave-based boundary value problem have been recently discussed in ref. [11] for predicting the response of an elastic structure under local force excitations. In this work, a numerical strategy has been proposed by which ill-conditioned problems, resulting from the wave representation of the local excitations, can be circumvented. It invokes both right and left eigenvectors of the symplectic transfer matrix relating a typical substructure, and uses the fact that they are orthogonal. The same strategy has been used in ref. [10]. It has been successfully employed for predicting the response of a clamped Euler-Bernoulli beam under transverse excitation as well as

the response of a simply supported Kirchhoff-Love plate under punctual force.

Apart from these works, a question arises whether the relevance of the WFE formalism holds when arbitrary Neumann-to-Dirichlet problems are addressed. The underlying numerical issue is that the resulting matrix forms are prone to large dissimilarities among their components as both wave displacement and wave force terms are invoked. This means that ill-conditioning is likely to occur. Another question arises whether the WFE method can be relevant for addressing the vibratory behavior of multi-layered systems involving both soft and stiff materials, since the wave components can be largely disparate over the whole cross-section. These problematics relate the motivation of the present work.

This study aims at applying the WFE method for describing the LF and MF vibratory behavior of arbitrary Neumann-to-Dirichlet problems. These can involve single and coupled beam-like structures with 2D complex spatial dynamics over their cross-section, as well as multi-layered systems involving soft and stiff materials. Also, it aims at discussing on the relevance of the numerical wave-based formulation through comparisons with reference solutions provided by the standard FE method, when the global discretized structure is computed.

The framework of the WFE method for computing the wave modes traveling along straight elastic structures is presented in Section 2. The computation of forced responses based on wave mode expansion is discussed in Section 3. Neumann-to-Dirichlet problems are addressed in Section 4. The resulting wave-based matrix forms are presented for two classes of problems, say a single waveguide and two waveguides coupled through an elastic junction. A strategy for circumventing ill-conditioned problems is presented, by which appropriate scalings are employed. The underlying numerical issues of the WFE formalism for addressing the forced response of multi-layered systems are discussed in Section 5. It is shown that the WFE method suffers from numerical instabilities and pollution

effects. A regularization strategy, by which the kinematic variables are expanded onto an alternative wave basis, is proposed to solve these issues. Emphasis is on the fact that this alternative wave-based formalism is quite general and can be applied, under appropriate assumptions, to other classes of problems like plates. The relevance of the regularization strategy is numerically highlighted compared with FE solutions.

Figure 1

2. The WFE method

2.1. Formulation of wave modes

The WFE method numerically provides the LF and MF wave propagation into periodic elastic systems [2]. In this framework, a given structure is assumed to be described numerically from a set of identical substructures. These are assumed to be modeled using the same FE model and connected along a principal axis — say axis x — referred to as the direction of propagation (see Figure 1). The length of each substructure, along this direction, is denoted as d . Assuming mesh compatibility at coupling interfaces between substructures provides the same nodal distribution over their left and right boundaries: in other words, each boundary is assumed to contain the same number of degrees of freedom (DOFs), say n . The WFE method is based on the dynamic equilibrium of one of these substructures (see Figure 1), which is classically formulated in the frequency domain as

$$\mathbf{D}\mathbf{q} = \mathbf{F}, \tag{1}$$

where \mathbf{q} and \mathbf{F} represent the displacements and forces, respectively; \mathbf{D} represents the dynamic stiffness operator of the substructure, expressed as $\mathbf{D} = -\omega^2\mathbf{M} + \mathbf{K}(1 + i\eta)$ where \mathbf{M} and \mathbf{K} are the mass and stiffness matrices, respectively, while

η is the loss factor and ω is the angular frequency. Following the theory of Zhong & Williams [3], the dynamic equilibrium equation (1) can be reformulated in terms of state vectors as

$$\mathbf{u}_R = \mathbf{S}\mathbf{u}_L, \quad (2)$$

where \mathbf{S} is a $(2n \times 2n)$ symplectic matrix, the subscripts L and R refer to as the left and right boundaries, while $\mathbf{u}_L^T = [(\mathbf{q}_L)^T \ (-\mathbf{F}_L)^T]$ and $\mathbf{u}_R^T = [(\mathbf{q}_R)^T \ (\mathbf{F}_R)^T]$. The full derivation of \mathbf{S} is expressed as:

$$\mathbf{S} = \left[\begin{array}{c|c} -(\mathbf{D}_{LR}^*)^{-1}\mathbf{D}_{LL}^* & -(\mathbf{D}_{LR}^*)^{-1} \\ \hline \mathbf{D}_{RL}^* - \mathbf{D}_{RR}^*(\mathbf{D}_{LR}^*)^{-1}\mathbf{D}_{LL}^* & -\mathbf{D}_{RR}^*(\mathbf{D}_{LR}^*)^{-1} \end{array} \right], \quad (3)$$

where \mathbf{D}^* refers to as the dynamic stiffness matrix of the substructure condensed onto its left and right boundaries. Using the coupling conditions between two consecutive substructures k and $k - 1$, say

$$\mathbf{u}_L^{(k)} = \mathbf{u}_R^{(k-1)}, \quad (4)$$

in Eq. (2) leads to [5]:

$$\mathbf{u}_L^{(k)} = \mathbf{S}\mathbf{u}_L^{(k-1)}. \quad (5)$$

Invoking Bloch's theorem [14], the solutions of Eq. (5) can be readily expressed as $\mathbf{u}_L^{(k)} = \mu\mathbf{u}_L^{(k-1)}$. These solutions are denoted as $\{(\mu_j, \Phi_j)\}_j$ and refer to as the wave modes traveling along the global structure. They are numerically computed by means of the following eigenvalue problem:

$$\mathbf{S}\Phi_j = \mu_j\Phi_j \quad , \quad \det(\mathbf{S} - \mu_j\mathbf{I}) = 0. \quad (6)$$

For a given mode j , the scalar parameter μ_j characterizes the wavenumber k_j as $\mu_j = \exp(-ik_jd)$, while the vectorial parameter Φ_j represents the wave shape,

which relates the spatial distribution of the displacements and internal forces over the cross-section. It is worth emphasizing that each eigenvector Φ_j can be split into wave displacement and wave force components as $\Phi_j^T = [(\Phi_q)_j^T (\Phi_F)_j^T]$. The wave shapes are interpolated from the trace of the FE discretization onto the substructure cross-section. This particularly means that the mesh density must be fine enough if MF behavior must be predicted, in the sense that a sufficient number of highly oscillating wave shapes must be computed for accurately spanning the cross-section dynamics.

Remark 1. As pointed out by Zhong & Williams [3], direct computation of the eigenvalue problem (6) can be prone to large sensitivities with regard to perturbation analysis. According to the Bauer-Fike theorem [15], the problem is that the eigenvector matrix of \mathbf{S} , namely Φ , can be ill-conditioned. This can be explained as it is partitioned into displacement and force components (see above) whose values can be largely disparate. To solve this issue, Zhong & Williams have proposed an homogeneous generalized eigenvalue problem of the following form:

$$\mathbf{N}\mathbf{w}_j = \mu_j \mathbf{L}\mathbf{w}_j \quad , \quad \det(\mathbf{N} - \mu_j \mathbf{L}) = 0, \quad (7)$$

where the eigenvectors $\{\mathbf{w}_j\}_j$ relate the displacements of the substructure only. This eigenvalue problem has been successfully used for addressing the wave propagation into elastic, elasto-acoustic and multi-layered systems [5, 6, 16]. It will be used in the framework of the paper so as to compute the wave modes $\{(\mu_j, \Phi_j)\}_j$. It is worth noting that Zhong & Williams have proposed a “better conditioned” form of the eigenvalue problem with double eigenvalues $\{\lambda_j\}_j$, such that $\lambda_j = \mu_j + 1/\mu_j \forall j$. These are associated to eigenvectors which come in pair as $\{(\mathbf{w}_j^1, \mathbf{w}_j^2)\}_j$; these are used to determine the wave modes $\{\mathbf{w}_j\}_j$ of the original problem (7) as $\mathbf{w}_j = \alpha_j^1 \mathbf{w}_j^1 + \alpha_j^2 \mathbf{w}_j^2 \forall j$ [10]. Notice that it is not clear whether this alterna-

tive form brings an optimal determination of the wave modes, given that singular problems can be encountered for determining the amplitudes $\{(\alpha_j^1, \alpha_j^2)\}_j$ (see ref. [17]).

Remark 2. Throughout the remainder of the paper, it will be assumed that the eigenvectors $\{\Phi_j\}_j$ are linearly independent when $\omega \neq 0$ [18]. This assumption occults the possibility of merging two wave modes of quite similar natures in a single one, which is coherent with the rule of wave mode conversion process in the frequency domain and the fact that two similar wave shapes cannot exhibit two different group velocities at the same frequency [19]. According to ref. [18], this assumption can break down when $\omega \rightarrow 0$, as the classic LF wave modes (say longitudinal, torsional, flexural, shearing) tend to share the same eigenvalue $\mu = 1$ — this is explained as rigid body motions take place — which is generally defective. In this sense, the eigenvalue problem may be prone to large sensitivities [20], e.g. with regard to slight discretization errors which can perturb the components of matrix \mathbf{S} .

2.2. Criteria for tracking the frequency evolution of wave modes

Tracking the frequency evolution of each wave mode is a crucial step of the WFE method. This brings insight into the frequency evolution of the structural behavior and leads to properly select among all the waves those which are the most contributing for computing the forced responses within a given frequency band. As opposed to the analytical formulations, the numerical approach provides wave modes at discrete frequencies. Correspondence among two sets of modes defined at two frequencies, close to each other, can be achieved nonetheless in the WFE framework using the following criterion [5]:

Given two wave modes j and m defined at angular frequency ω , such that

$\mu_m(\omega) = 1/\mu_j(\omega)$, and for sufficiently small Δ_ω , wave mode j defined at angular frequency $\omega + \Delta_\omega$ is such that:

$$\left| \frac{\Phi_m(\omega)^T \mathbf{J} \Phi_j(\omega + \Delta_\omega)}{\|\Phi_m(\omega)\| \|\Phi_j(\omega + \Delta_\omega)\|} \right| = \max_k \left\{ \left| \frac{\Phi_m(\omega)^T \mathbf{J} \Phi_k(\omega + \Delta_\omega)}{\|\Phi_m(\omega)\| \|\Phi_k(\omega + \Delta_\omega)\|} \right| \right\}, \quad (8)$$

where $\|\mathbf{v}\|$ denotes the hermitian norm of a vector \mathbf{v} , defined as $\|\mathbf{v}\| = \sqrt{\mathbf{v}^H \mathbf{v}}$ where H denotes the conjugate transpose. This criterion is based on the symplectic orthogonality property of the matrix \mathbf{S} (cf. Eq. (2)), which states that

$$\Phi_j^T \mathbf{J} \Phi_l = 0 \quad \text{for } \mu_j \neq 1/\mu_l \quad \text{where} \quad \mathbf{J} = \begin{bmatrix} \mathbf{0} & \mathbf{I} \\ -\mathbf{I} & \mathbf{0} \end{bmatrix}. \quad (9)$$

Using the partitioning $\Phi_j^T = [(\Phi_q)_j^T (\Phi_F)_j^T]$, the symplectic orthogonality (9) can be readily written as $(\Phi_F)_l^T (\Phi_q)_j - (\Phi_F)_j^T (\Phi_q)_l = 0$ (for $\mu_j \neq 1/\mu_l$). It has been shown in ref. [21] that this constitutes a necessary requirement to satisfy the Maxwell-Betti reciprocity theorem into an elastic waveguide, considering the wave modes Φ_j and Φ_l as two states of excitations and induced displacements.

The criterion (8) breaks down unfortunately for very low frequencies given that eigenvalues $\{\mu\}_j$ can be extremely close to each other. This means that orthogonality properties among modes are not necessarily verified numerically. The following criterion based on the hermitian scalar product can be used instead [16]:

Given wave mode j defined at angular frequency ω and for sufficiently small Δ_ω , wave mode j defined at angular frequency $\omega + \Delta_\omega$ is such that:

$$\left| \frac{\Phi_j(\omega)^H \Phi_j(\omega + \Delta_\omega)}{\|\Phi_j(\omega)\| \|\Phi_j(\omega + \Delta_\omega)\|} \right| = \max_k \left\{ \left| \frac{\Phi_j(\omega)^H \Phi_k(\omega + \Delta_\omega)}{\|\Phi_j(\omega)\| \|\Phi_k(\omega + \Delta_\omega)\|} \right| \right\}. \quad (10)$$

This criterion is well known as Modal Assurance Criterion (MAC) and is used for estimating the correlation among wave shapes. This criterion is expected to be less accurate compared to Eq. (8) since orthogonality properties are not invoked, unless frequency step Δ_ω is chosen small enough. However, it appears more general in

the sense that it can be applied for tracking the eigensolutions of a matrix which is not necessarily symplectic (see ref. [16]).

2.3. Relationships between incident and reflected modes

It is well established that there exists the same number n of *incident* and *reflected* modes ¹ traveling along a straight structure [3] (see Figure 1), where n represents the number of DOFs contained onto the left or right boundary of the considered substructure. In this sense, the wave basis $\{\Phi_j\}_j$ can be expressed in matrix form as

$$\Phi = \begin{bmatrix} \Phi_{\mathbf{q}}^{\text{inc}} & \Phi_{\mathbf{q}}^{\text{ref}} \\ \Phi_{\mathbf{F}}^{\text{inc}} & \Phi_{\mathbf{F}}^{\text{ref}} \end{bmatrix}, \quad (11)$$

where $\Phi_{\mathbf{q}}^{\text{inc}}$, $\Phi_{\mathbf{F}}^{\text{inc}}$, $\Phi_{\mathbf{q}}^{\text{ref}}$ and $\Phi_{\mathbf{F}}^{\text{ref}}$ are square ($n \times n$) matrices; the superscripts *inc* and *ref* refer to as incident and reflected waves while the subscripts \mathbf{q} and \mathbf{F} refer to as displacement and force components. Accounting for the symmetry of the wave propagation problem with respect to any transversal plane (y, z) (cf. Figure 1), it is readily established that reflected and incident modes are linked through the following rules [22, 8]:

$$\boldsymbol{\mu}^{\text{ref}} = (\boldsymbol{\mu}^{\text{inc}})^{-1}, \quad (12)$$

and

$$\Phi_{\mathbf{q}}^{\text{ref}} = \mathcal{R}\Phi_{\mathbf{q}}^{\text{inc}} \quad , \quad \Phi_{\mathbf{F}}^{\text{ref}} = -\mathcal{R}\Phi_{\mathbf{F}}^{\text{inc}}. \quad (13)$$

In Eq. (12), $\boldsymbol{\mu}^{\text{inc}}$ and $\boldsymbol{\mu}^{\text{ref}}$ represent the diagonal eigenvalue matrices of the incident and reflected modes, respectively. Eq. (12) is commonly used in the literature

¹In the framework of this paper, they refer to as (by convention) the waves traveling in the positive and negative directions.

(see for instance [10, 9]) and means that dual incident and reflected modes reveal eigenvalues which are inverse, one compared to the other. Without loss of generality, as the elastic system is dissipative, incident and reflected eigenvalues can be classified as $\{\mu_j^{\text{inc}}\}_{j=1,\dots,n} = \{\mu_j : |\mu_j| < 1\}_j$ and $\{\mu_j^{\text{ref}}\}_{j=1,\dots,n} = \{\mu_j : |\mu_j| > 1\}_j$ or *vice versa* [5]. On the other hand, in Eq. (13), \mathcal{R} is the diagonal symmetry transformation matrix; the minus sign on the right hand side of the second term of Eq. (13) results from the state vector representation which is quite different for the symmetric problem as left and right boundaries appear inverted. Eq. (13) enforces the coherence between incident and reflected modes, in the sense that the equalities $\|(\Phi_{\mathbf{q}}^{\text{inc}})_j\| = \|(\Phi_{\mathbf{q}}^{\text{ref}})_j\|$ and $\|(\Phi_{\mathbf{F}}^{\text{inc}})_j\| = \|(\Phi_{\mathbf{F}}^{\text{ref}})_j\|$ are verified $\forall j$, while it is not sure whether these relations can be perfectly transcribed through the eigenvalue problem (6) only, since the latter can be prone to numerical dispersion. This can cause drastic problems for predicting the forced response of the global structure (see Section 4.3.1).

Proposition 1. Each of the families $\{(\Phi_{\mathbf{q}}^{\text{inc}})_j\}_{j=1,\dots,n}$, $\{(\Phi_{\mathbf{q}}^{\text{ref}})_j\}_{j=1,\dots,n}$, $\{(\Phi_{\mathbf{F}}^{\text{inc}})_j\}_{j=1,\dots,n}$ and $\{(\Phi_{\mathbf{F}}^{\text{ref}})_j\}_{j=1,\dots,n}$ represents linearly independent vectors.

Proof. According to ref. [10], the eigenvalues $\{\mu_j^{\text{inc}}\}_j$ and $\{\mu_j^{\text{ref}} : \mu_j^{\text{ref}} = 1/\mu_j^{\text{inc}}\}_j$ are solutions of a quadratic eigenvalue problem of dimension n , which is formulated by means of the wave displacement components $\{(\Phi_{\mathbf{q}}^{\text{inc}})_j\}_j$ only. For $(\Phi_{\mathbf{q}}^{\text{inc}})_k$ given, this yields the following two equations [10]:

$$[\mathbf{D}_{\text{RL}}^* + (\mathbf{D}_{\text{LL}}^* + \mathbf{D}_{\text{RR}}^*)\mu_k^{\text{inc}} + \mathbf{D}_{\text{LR}}^*(\mu_k^{\text{inc}})^2](\Phi_{\mathbf{q}}^{\text{inc}})_k = \mathbf{0}, \quad (14)$$

and

$$(\Phi_{\mathbf{q}}^{\text{inc}})_k^T [\mathbf{D}_{\text{RL}}^* + (\mathbf{D}_{\text{LL}}^* + \mathbf{D}_{\text{RR}}^*)\mu_k^{\text{ref}} + \mathbf{D}_{\text{LR}}^*(\mu_k^{\text{ref}})^2] = \mathbf{0}^T, \quad (15)$$

where it has been taken into account that $\mathbf{D}_{\text{LR}}^* = (\mathbf{D}_{\text{RL}}^*)^T$ and $\mathbf{D}_{\text{LL}}^* + \mathbf{D}_{\text{RR}}^* = (\mathbf{D}_{\text{LL}}^* + \mathbf{D}_{\text{RR}}^*)^T$. This enables μ_k^{inc} and μ_k^{ref} to represent the solutions of a single quadratic equation:

$$(\Phi_{\mathbf{q}}^{\text{inc}})_k^T [\mathbf{D}_{\text{RL}}^* + (\mathbf{D}_{\text{LL}}^* + \mathbf{D}_{\text{RR}}^*)\mu + \mathbf{D}_{\text{LR}}^*\mu^2](\Phi_{\mathbf{q}}^{\text{inc}})_k = 0. \quad (16)$$

Finally note that wave force and wave displacement components are linked as [10]:

$$(\Phi_{\mathbf{F}})_j = [\mathbf{D}_{\text{LL}}^* + \mathbf{D}_{\text{LR}}^*\mu_j](\Phi_{\mathbf{q}})_j \quad \forall j. \quad (17)$$

To prove that $\{(\Phi_{\mathbf{q}}^{\text{inc}})_j\}_j$ are linearly independent, let us consider for simplicity one hypothetical vector $(\Phi_{\mathbf{q}}^{\text{inc}})_l$ where $l \neq k$ and such that $(\Phi_{\mathbf{q}}^{\text{inc}})_l = \alpha(\Phi_{\mathbf{q}}^{\text{inc}})_k$ ($\alpha \neq 0$). It is readily verified that the pair of eigenvalues $(\mu_l^{\text{inc}}, \mu_l^{\text{ref}})$ satisfies Eq. (16). This necessarily yields $\mu_l^{\text{inc}} = \mu_k^{\text{inc}}$ and $\mu_l^{\text{ref}} = \mu_k^{\text{ref}}$ ², taking into account that both μ_k^{inc} and μ_k^{ref} are the two solutions of Eq. (16). This also yields $(\Phi_{\mathbf{F}}^{\text{inc}})_l = \alpha(\Phi_{\mathbf{F}}^{\text{inc}})_k$, considering Eq. (17). This generalizes the linear dependency as $\Phi_l^{\text{inc}} = \alpha\Phi_k^{\text{inc}}$ for two incident eigenvectors l and k of matrix \mathbf{S} , which is contradictory to the statement that $\{\Phi_j\}_j$ are linearly independent (see Remark 2). Thus, the vectors $\{(\Phi_{\mathbf{q}}^{\text{inc}})_j\}_j$ are linearly independent. A similar statement can be readily deduced for $\{(\Phi_{\mathbf{F}}^{\text{inc}})_j\}_j$, using Eq. (17). The proof that $\{(\Phi_{\mathbf{q}}^{\text{ref}})_j\}_j$, as well as $\{(\Phi_{\mathbf{F}}^{\text{ref}})_j\}_j$, are linearly independent can be easily deduced from the preceding derivation. \square

Proposition 2. Let us consider two sets of eigenvectors $\{\tilde{\Phi}_j^{\text{inc}}\}_{j=1,\dots,m}$ and $\{\tilde{\Phi}_j^{\text{ref}}\}_{j=1,\dots,m}$ extracted from the full families $\{\Phi_j^{\text{inc}}\}_{j=1,\dots,n}$ and $\{\Phi_j^{\text{ref}}\}_{j=1,\dots,n}$, where $m \leq n$, and whose respective wave displacement and wave force components admit the following $(n \times m)$ matrix forms $\tilde{\Phi}_{\mathbf{q}}^{\text{inc}}$, $\tilde{\Phi}_{\mathbf{q}}^{\text{ref}}$, $\tilde{\Phi}_{\mathbf{F}}^{\text{inc}}$ and $\tilde{\Phi}_{\mathbf{F}}^{\text{ref}}$. Then,

²The case $\mu_l^{\text{inc}} = \mu_k^{\text{ref}}$ and $\mu_l^{\text{ref}} = \mu_k^{\text{inc}}$ can not occur if the following convention is retained [5]: $\{\mu_j^{\text{inc}}\}_j = \{\mu_j : |\mu_j| < 1\}_j$ and $\{\mu_j^{\text{ref}}\}_j = \{\mu_j : |\mu_j| > 1\}_j$ or *vice versa*.

the pseudo-inverse \mathbf{A}^+ of each of these matrices (each of them being termed as \mathbf{A}) can be computed as [15]:

$$\mathbf{A}^+ = [\mathbf{A}^H \mathbf{A}]^{-1} \mathbf{A}^H. \quad (18)$$

Proof. The proof follows directly from Proposition 1, taking into account that each of the matrices $\tilde{\Phi}_q^{\text{inc}}$, $\tilde{\Phi}_q^{\text{ref}}$, $\tilde{\Phi}_F^{\text{inc}}$ and $\tilde{\Phi}_F^{\text{ref}}$ is full column rank ($\text{rank}(\mathbf{A}) = m$). This yields the expected form of the pseudo-inverse [15]. \square

3. Wave mode expansion

The problem of predicting the harmonic response of a structure composed of N identical substructures is addressed (see Figure 1). In the WFE framework, the state vectors $\mathbf{u}_L^{(k)}$ and $\mathbf{u}_R^{(k)}$ — namely, the kinematic variables of a typical substructure k — are expanded onto a reduced wave basis $\{\tilde{\Phi}_j\}_j = \{\tilde{\Phi}_j^{\text{inc}}\}_{j=1,\dots,m} \cup \{\tilde{\Phi}_j^{\text{ref}}\}_{j=1,\dots,m}$, where $m \leq n$. This results in

$$\mathbf{u}_L^{(k)} = \tilde{\Phi}^{\text{inc}} \tilde{\mathbf{Q}}^{\text{inc}(k)} + \tilde{\Phi}^{\text{ref}} \tilde{\mathbf{Q}}^{\text{ref}(k)} \quad k = 1, \dots, N, \quad (19)$$

$$\mathbf{u}_R^{(k)} = \tilde{\Phi}^{\text{inc}} \tilde{\mathbf{Q}}^{\text{inc}(k+1)} + \tilde{\Phi}^{\text{ref}} \tilde{\mathbf{Q}}^{\text{ref}(k+1)} \quad k = 1, \dots, N, \quad (20)$$

where $\tilde{\Phi}^{\text{inc}}$ and $\tilde{\Phi}^{\text{ref}}$ are the $(2n \times m)$ matrix forms of the incident and reflected wave mode shapes, while $\tilde{\mathbf{Q}}^{\text{inc}}$ and $\tilde{\mathbf{Q}}^{\text{ref}}$ are the $(m \times 1)$ vector forms of the resulting modal amplitudes.

Remark 3. The reduced basis $\{\tilde{\Phi}_j\}_j$ is supposed to include the modes which mostly contribute to the forced response of the structure. Despite no rigorous criterion for selecting these modes, a simple strategy consists in constructing the wave basis from the standard LF propagating modes and the modes which either become

or are close to becoming propagating behind a certain limiting frequency [10].

Proposition 3. The spatial distribution of the modal amplitudes is governed as:

$$\tilde{\mathbf{Q}}^{\text{inc}(k)} = \tilde{\boldsymbol{\mu}}^{k-1} \tilde{\mathbf{Q}}^{\text{inc}(1)} \quad k = 1, \dots, N + 1, \quad (21)$$

$$\tilde{\mathbf{Q}}^{\text{ref}(k)} = \tilde{\boldsymbol{\mu}}^{-(k-1)} \tilde{\mathbf{Q}}^{\text{ref}(1)} \quad k = 1, \dots, N + 1, \quad (22)$$

where $\tilde{\boldsymbol{\mu}}$ represents the $(m \times m)$ diagonal eigenvalue matrix of the incident modes, which is such that $\tilde{\boldsymbol{\mu}} = \tilde{\boldsymbol{\mu}}^{\text{inc}} = (\tilde{\boldsymbol{\mu}}^{\text{ref}})^{-1}$ (cf. Eq. (12)).

Proof. Inserting Eqs. (19) and (20) into $\mathbf{u}_R^{(k-1)} = \mathbf{S}^{k-1} \mathbf{u}_L^1$ — provided by the recurrence equation (5) and the coupling conditions (4) — and given that $\mathbf{S}^{k-1} \tilde{\boldsymbol{\Phi}}^{\text{inc}} = \tilde{\boldsymbol{\Phi}}^{\text{inc}} \tilde{\boldsymbol{\mu}}^{k-1}$ and $\mathbf{S}^{k-1} \tilde{\boldsymbol{\Phi}}^{\text{ref}} = \tilde{\boldsymbol{\Phi}}^{\text{ref}} \tilde{\boldsymbol{\mu}}^{-(k-1)}$ leads to

$$\tilde{\boldsymbol{\Phi}}^{\text{inc}} \tilde{\mathbf{Q}}^{\text{inc}(k)} + \tilde{\boldsymbol{\Phi}}^{\text{ref}} \tilde{\mathbf{Q}}^{\text{ref}(k)} = \tilde{\boldsymbol{\Phi}}^{\text{inc}} \tilde{\boldsymbol{\mu}}^{k-1} \tilde{\mathbf{Q}}^{\text{inc}(1)} + \tilde{\boldsymbol{\Phi}}^{\text{ref}} \tilde{\boldsymbol{\mu}}^{-(k-1)} \tilde{\mathbf{Q}}^{\text{ref}(1)}. \quad (23)$$

Left multiplying Eq. (23) either by $(\tilde{\boldsymbol{\Phi}}^{\text{ref}})^T \mathbf{J}$ or by $(\tilde{\boldsymbol{\Phi}}^{\text{inc}})^T \mathbf{J}$, and accounting for the symplectic orthogonality property (9) — which state that $(\tilde{\boldsymbol{\Phi}}^{\text{ref}})^T \mathbf{J} \tilde{\boldsymbol{\Phi}}^{\text{ref}} = \mathbf{0}$ and $(\tilde{\boldsymbol{\Phi}}^{\text{inc}})^T \mathbf{J} \tilde{\boldsymbol{\Phi}}^{\text{inc}} = \mathbf{0}$ ³ — finally leads to Eqs. (21) and (22). \square

The wave-based boundary value problem is constituted from the governing equations (21), (22) and the boundary conditions. These can be formulated in a general way as [23, 5]:

$$\tilde{\mathbf{Q}}^{\text{ref}}|_{\text{lim}} = \tilde{\mathbb{C}} \tilde{\mathbf{Q}}^{\text{inc}}|_{\text{lim}} + \tilde{\mathcal{F}}, \quad (24)$$

where $\tilde{\mathbb{C}}$ refers to as the diffusion matrix and provides the reflection and transmission coefficients of the wave modes across a given boundary, while the vector $\tilde{\mathcal{F}}$

³Note that $(\tilde{\boldsymbol{\Phi}}^{\text{ref}})^T \mathbf{J} \tilde{\boldsymbol{\Phi}}^{\text{inc}}$ and $(\tilde{\boldsymbol{\Phi}}^{\text{inc}})^T \mathbf{J} \tilde{\boldsymbol{\Phi}}^{\text{ref}}$ are diagonal matrices.

reflects the excitation sources. It has been established in ref. [23] that Eq. (24) is well suited for describing the Neumann and Dirichlet boundary conditions. These write as

$$[\mathbf{0}|\mathbf{I}] \mathbf{u} = \pm \mathbf{F}_0, \quad (\text{Neumann condition}) \quad (25)$$

$$[\mathbf{I}|\mathbf{0}] \mathbf{u} = \mathbf{q}_0, \quad (\text{Dirichlet condition}) \quad (26)$$

and can be expanded onto the wave basis $\{\tilde{\Phi}_j\}_j$ (see above) to give

$$\tilde{\Phi}_F^{\text{inc}} \tilde{\mathbf{Q}}^{\text{inc}} + \tilde{\Phi}_F^{\text{ref}} \tilde{\mathbf{Q}}^{\text{ref}} = \pm \mathbf{F}_0, \quad (\text{Neumann condition}) \quad (27)$$

$$\tilde{\Phi}_q^{\text{inc}} \tilde{\mathbf{Q}}^{\text{inc}} + \tilde{\Phi}_q^{\text{ref}} \tilde{\mathbf{Q}}^{\text{ref}} = \mathbf{q}_0. \quad (\text{Dirichlet condition}) \quad (28)$$

It is worth emphasizing that the sign ahead \mathbf{F}_0 in Eq. (27) is negative if the left boundary is concerned (this is explained as the state vector representation writes $\mathbf{u}_L^T = [(\mathbf{q}_L)^T \ (-\mathbf{F}_L)^T]$) whilst it is positive if the right boundary is studied (in this case, the state vector representation writes $\mathbf{u}_R^T = [(\mathbf{q}_R)^T \ (\mathbf{F}_R)^T]$). Left multiplying Eqs. (27) and (28) by the left pseudo-inverses $(\tilde{\Phi}_F^{\text{ref}})^+$ and $(\tilde{\Phi}_q^{\text{ref}})^+$ (see Proposition 2), respectively, leads to the form of Eq. (24), as expected.

Remark 4. As pointed out in Remark 2, the wave mode expansion provided by Eqs. (19) and (20) may be inaccurate when $\omega \rightarrow 0$, that is for very low frequencies. Here, a part of the wave modes — namely the classic LF modes — tend to be linearly dependent, meaning that the numerical wave-based boundary value problem reveals poor conditioning.

Summarizing, the wave-based boundary value problem is formulated from Eqs. (21), (22), and the boundary conditions, which can be formulated in a general way by Eq. (24) or more specifically by Eqs. (27) and (28). Solving the wave-based boundary value problem consists in finding, for instance, the modal amplitudes

$\tilde{\mathbf{Q}}^{\text{inc}(1)}$ and $\tilde{\mathbf{Q}}^{\text{ref}(1)}$ for the left cross-section of the global structure. Thus, the spatial distribution of the modal amplitudes, along the structure, are provided by means of Eqs. (21) and (22), while the spatial distribution of the kinematic variables (say, displacements and internal forces) are provided by means of Eqs. (19) and (20). The wave-based solutions are expected to be in accordance with the results provided by the standard FE method, which requires the computation of the full discretized structure with N connected substructures. Compared to the FE method, the WFE method yields a large decrease of the CPU times for calculating the LF and MF forced responses, as it involves numerical models of small dimension (i.e. twice the number of retained wave modes). Another feature of the method is its large flexibility for addressing several classes of problems involving single as well as coupled straight systems with arbitrary conditions, when the wave modes for one or few substructures have been computed once and for all.

4. The Neumann-to-Dirichlet problem

4.1. Single waveguide

The problem of a single waveguide — say for instance a beam-like structure —, whose left and right ends are respectively submitted to prescribed forces and displacements, is addressed (cf. Figure 2 for instance). In this case, the boundary conditions write (cf. Eqs. (27) and (28)):

$$\tilde{\Phi}_{\mathbf{F}}^{\text{inc}} \tilde{\mathbf{Q}}^{\text{inc}(1)} + \tilde{\Phi}_{\mathbf{F}}^{\text{ref}} \tilde{\mathbf{Q}}^{\text{ref}(1)} = -\mathbf{F}_0, \quad (29)$$

$$\tilde{\Phi}_{\mathbf{q}}^{\text{inc}} \tilde{\mathbf{Q}}^{\text{inc}(N+1)} + \tilde{\Phi}_{\mathbf{q}}^{\text{ref}} \tilde{\mathbf{Q}}^{\text{ref}(N+1)} = \mathbf{q}_0. \quad (30)$$

where N is the number of FE substructures considered to discretize the global system. Accounting for the governing equations (21) and (22) yields

$$\tilde{\Phi}_F^{\text{inc}} \tilde{\mathbf{Q}}^{\text{inc}(1)} + \tilde{\Phi}_F^{\text{ref}} \tilde{\mathbf{Q}}^{\text{ref}(1)} = -\mathbf{F}_0, \quad (31)$$

$$\tilde{\Phi}_q^{\text{inc}} \tilde{\mu}^N \tilde{\mathbf{Q}}^{\text{inc}(1)} + \tilde{\Phi}_q^{\text{ref}} \tilde{\mu}^{-N} \tilde{\mathbf{Q}}^{\text{ref}(1)} = \mathbf{q}_0, \quad (32)$$

which, in matrix form, results in

$$\begin{bmatrix} \tilde{\Phi}_F^{\text{inc}} & \tilde{\Phi}_F^{\text{ref}} \\ \tilde{\Phi}_q^{\text{inc}} \tilde{\mu}^N & \tilde{\Phi}_q^{\text{ref}} \tilde{\mu}^{-N} \end{bmatrix} \begin{pmatrix} \tilde{\mathbf{Q}}^{\text{inc}(1)} \\ \tilde{\mathbf{Q}}^{\text{ref}(1)} \end{pmatrix} = \begin{pmatrix} -\mathbf{F}_0 \\ \mathbf{q}_0 \end{pmatrix}. \quad (33)$$

Direct inversion of the matrix in Eq. (33) can suffer from nearly singular problems. This is explained as the ratios between the diagonal components of matrices $\tilde{\mu}^{-N}$ and $\tilde{\mu}^N$, as well as the ratios between the components of $\tilde{\Phi}_q$ and $\tilde{\Phi}_F$, can reveal extremely large values. This issue can be circumvented using appropriate scalings [15] as:

$$\begin{aligned} & \begin{bmatrix} \mathbf{I} & (\tilde{\Phi}_F^{\text{inc}})^+ \tilde{\Phi}_F^{\text{ref}} \tilde{\mu}^N \\ (\tilde{\Phi}_q^{\text{ref}})^+ \tilde{\Phi}_q^{\text{inc}} \tilde{\mu}^N & \mathbf{I} \end{bmatrix} \begin{bmatrix} \mathbf{I} & \mathbf{0} \\ \mathbf{0} & \tilde{\mu}^{-N} \end{bmatrix} \begin{pmatrix} \tilde{\mathbf{Q}}^{\text{inc}(1)} \\ \tilde{\mathbf{Q}}^{\text{ref}(1)} \end{pmatrix} \\ & = \begin{pmatrix} -(\tilde{\Phi}_F^{\text{inc}})^+ \mathbf{F}_0 \\ (\tilde{\Phi}_q^{\text{ref}})^+ \mathbf{q}_0 \end{pmatrix}. \end{aligned} \quad (34)$$

The system provided by (34) can be solved without difficulty since the first matrix on the left hand side appears well conditioned (it is worth noting that the eigenvalue matrix of the incident modes $\tilde{\mu}$ is such that $\|\tilde{\mu}\|_{\max} < 1$) while the second matrix is diagonal. In the present form, the diagonal matrix $\tilde{\mu}^N$ is multiplied either with the matrix $(\tilde{\Phi}_F^{\text{inc}})^+ \tilde{\Phi}_F^{\text{ref}}$ or with the matrix $(\tilde{\Phi}_q^{\text{ref}})^+ \tilde{\Phi}_q^{\text{inc}}$, which results in a filtering effect for high order modes whose highly fluctuating cross-section dynamics can be sources of numerical instabilities. In other words, the contribution of high order modes in the computation of $(\tilde{\Phi}_F^{\text{inc}})^+ \tilde{\Phi}_F^{\text{ref}}$ and $(\tilde{\Phi}_q^{\text{ref}})^+ \tilde{\Phi}_q^{\text{inc}}$ are lowered given

that they are scaled down using close to zero terms $\{\mu_j^N\}_{j \geq p}$ (this is explained as $|\mu_j| < 1 \forall j$ and N can be large). Solving Eq. (34) finally gives

$$\begin{aligned} & \begin{pmatrix} \tilde{\mathbf{Q}}^{\text{inc}(1)} \\ \tilde{\mathbf{Q}}^{\text{ref}(1)} \end{pmatrix} \\ &= \begin{bmatrix} \mathbf{I} & \mathbf{0} \\ \mathbf{0} & \tilde{\mu}^N \end{bmatrix} \begin{bmatrix} \mathbf{I} & (\tilde{\Phi}_F^{\text{inc}})^+ \tilde{\Phi}_F^{\text{ref}} \tilde{\mu}^N \\ (\tilde{\Phi}_q^{\text{ref}})^+ \tilde{\Phi}_q^{\text{inc}} \tilde{\mu}^N & \mathbf{I} \end{bmatrix}^{-1} \begin{pmatrix} -(\tilde{\Phi}_F^{\text{inc}})^+ \mathbf{F}_0 \\ (\tilde{\Phi}_q^{\text{ref}})^+ \mathbf{q}_0 \end{pmatrix} \end{aligned} \quad (35)$$

Remark 5. The strategy used for solving the Neumann-to-Dirichlet problem can be adapted without difficulty so as to address the Neumann problem or the Dirichlet problem, say for instance a beam-like structure whose left and right ends are either respectively submitted to prescribed force vectors \mathbf{F}_0 and \mathbf{F}'_0 or respectively submitted to prescribed displacement vectors \mathbf{q}_0 and \mathbf{q}'_0 . This requires in Eq. (35) the subscript q to be switched with F or *vice versa*, and the appropriate boundary conditions to be included. This results in:

- *For the Neumann problem:*

$$\begin{aligned} & \begin{pmatrix} \tilde{\mathbf{Q}}^{\text{inc}(1)} \\ \tilde{\mathbf{Q}}^{\text{ref}(1)} \end{pmatrix} \\ &= \begin{bmatrix} \mathbf{I} & \mathbf{0} \\ \mathbf{0} & \tilde{\mu}^N \end{bmatrix} \begin{bmatrix} \mathbf{I} & (\tilde{\Phi}_F^{\text{inc}})^+ \tilde{\Phi}_F^{\text{ref}} \tilde{\mu}^N \\ (\tilde{\Phi}_F^{\text{ref}})^+ \tilde{\Phi}_F^{\text{inc}} \tilde{\mu}^N & \mathbf{I} \end{bmatrix}^{-1} \begin{pmatrix} -(\tilde{\Phi}_F^{\text{inc}})^+ \mathbf{F}_0 \\ (\tilde{\Phi}_F^{\text{ref}})^+ \mathbf{F}'_0 \end{pmatrix} \end{aligned} \quad (36)$$

- *For the Dirichlet problem:*

$$\begin{aligned} & \begin{pmatrix} \tilde{\mathbf{Q}}^{\text{inc}(1)} \\ \tilde{\mathbf{Q}}^{\text{ref}(1)} \end{pmatrix} \\ &= \begin{bmatrix} \mathbf{I} & \mathbf{0} \\ \mathbf{0} & \tilde{\mu}^N \end{bmatrix} \begin{bmatrix} \mathbf{I} & (\tilde{\Phi}_q^{\text{inc}})^+ \tilde{\Phi}_q^{\text{ref}} \tilde{\mu}^N \\ (\tilde{\Phi}_q^{\text{ref}})^+ \tilde{\Phi}_q^{\text{inc}} \tilde{\mu}^N & \mathbf{I} \end{bmatrix}^{-1} \begin{pmatrix} (\tilde{\Phi}_q^{\text{inc}})^+ \mathbf{q}_0 \\ (\tilde{\Phi}_q^{\text{ref}})^+ \mathbf{q}'_0 \end{pmatrix} \end{aligned} \quad (37)$$

4.2. Two coupled waveguides

The problem of two waveguides — namely waveguide 1 and waveguide 2 — coupled through a *non excited* elastic junction is addressed. The junction can be arbitrary and can reveal a complex behavior, *a priori*. In previous works [5, 24], it has been established that the amplitudes of the modes reflected by – and incident to – the coupling element can be linked as:

$$\begin{pmatrix} \tilde{\mathbf{Q}}_{\text{wg1}}^{\text{ref}} \\ \tilde{\mathbf{Q}}_{\text{wg2}}^{\text{ref}} \end{pmatrix} = \begin{bmatrix} \tilde{\mathbb{C}}_{11} & \tilde{\mathbb{C}}_{12} \\ \tilde{\mathbb{C}}_{21} & \tilde{\mathbb{C}}_{22} \end{bmatrix} \begin{pmatrix} \tilde{\mathbf{Q}}_{\text{wg1}}^{\text{inc}} \\ \tilde{\mathbf{Q}}_{\text{wg2}}^{\text{inc}} \end{pmatrix}, \quad (38)$$

where `wg1` and `wg2` refer to as waveguide 1 and waveguide 2, respectively; $\{\tilde{\mathbb{C}}_{ij}\}_{ij}$ represent the square block components of the diffusion matrix $\tilde{\mathbb{C}}$, whose expression can be found in ref. [5]. On their uncoupled limits, the waveguides 1 and 2 are assumed to be submitted to prescribed forces and displacements, respectively. Summarizing, the boundary conditions are expressed as:

- *For waveguide 1:*

$$(\tilde{\Phi}_{\mathbf{F}}^{\text{inc}})_{\text{wg1}} \tilde{\mathbf{Q}}_{\text{wg1}}^{\text{inc}(1)} + (\tilde{\Phi}_{\mathbf{F}}^{\text{ref}})_{\text{wg1}} \tilde{\mathbf{Q}}_{\text{wg1}}^{\text{ref}(1)} = -\mathbf{F}_0, \quad (39)$$

$$\tilde{\mathbf{Q}}_{\text{wg1}}^{\text{ref}(N_1+1)} = \tilde{\mathbb{C}}_{11} \tilde{\mathbf{Q}}_{\text{wg1}}^{\text{inc}(N_1+1)} + \tilde{\mathbb{C}}_{12} \tilde{\mathbf{Q}}_{\text{wg2}}^{\text{inc}(N_2+1)}. \quad (40)$$

- *For waveguide 2:*

$$\tilde{\mathbf{Q}}_{\text{wg2}}^{\text{ref}(N_2+1)} = \tilde{\mathbb{C}}_{22} \tilde{\mathbf{Q}}_{\text{wg2}}^{\text{inc}(N_2+1)} + \tilde{\mathbb{C}}_{21} \tilde{\mathbf{Q}}_{\text{wg1}}^{\text{inc}(N_1+1)}, \quad (41)$$

$$(\tilde{\Phi}_{\mathbf{q}}^{\text{inc}})_{\text{wg2}} \tilde{\mathbf{Q}}_{\text{wg2}}^{\text{inc}(1)} + (\tilde{\Phi}_{\mathbf{q}}^{\text{ref}})_{\text{wg2}} \tilde{\mathbf{Q}}_{\text{wg2}}^{\text{ref}(1)} = \mathbf{q}_0, \quad (42)$$

where N_1 and N_2 represent the numbers of substructures constituting the waveguides 1 and 2, respectively. Accounting for the governing equations (21) and (22),

these boundary conditions can be expressed in matrix form as:

$$\left[\begin{array}{cc|cc} (\tilde{\Phi}_F^{\text{inc}})_{\text{wg1}} & (\tilde{\Phi}_F^{\text{ref}})_{\text{wg1}} & \mathbf{0} & \mathbf{0} \\ -\tilde{C}_{11}\tilde{\mu}_{\text{wg1}}^{N_1} & \tilde{\mu}_{\text{wg1}}^{-N_1} & \mathbf{0} & -\tilde{C}_{12}\tilde{\mu}_{\text{wg2}}^{N_2} \\ \hline -\tilde{C}_{21}\tilde{\mu}_{\text{wg1}}^{N_1} & \mathbf{0} & \tilde{\mu}_{\text{wg2}}^{-N_2} & -\tilde{C}_{22}\tilde{\mu}_{\text{wg2}}^{N_2} \\ \mathbf{0} & \mathbf{0} & (\tilde{\Phi}_q^{\text{ref}})_{\text{wg2}} & (\tilde{\Phi}_q^{\text{inc}})_{\text{wg2}} \end{array} \right] \begin{pmatrix} \tilde{Q}_{\text{wg1}}^{\text{inc}(1)} \\ \tilde{Q}_{\text{wg1}}^{\text{ref}(1)} \\ \tilde{Q}_{\text{wg2}}^{\text{ref}(1)} \\ \tilde{Q}_{\text{wg2}}^{\text{inc}(1)} \end{pmatrix} = \begin{pmatrix} -\mathbf{F}_0 \\ \mathbf{0} \\ \mathbf{0} \\ \mathbf{q}_0 \end{pmatrix}. \quad (43)$$

As was emphasized in the previous subsection, direct inversion of the matrix term in Eq. (43) may be prone to nearly singular problems. This is explained because, for each waveguide i , the diagonal components of matrices $\tilde{\mu}_{\text{wgi}}^{-N_i}$ and $\tilde{\mu}_{\text{wgi}}^{N_i}$, as well as the components of $(\tilde{\Phi}_{\text{wgi}})_q$ and $(\tilde{\Phi}_{\text{wgi}})_F$, can be strongly disparate. Again, appropriate scalings can be carried out for treating these problems. This gives:

$$\left[\begin{array}{cc|cc} \mathbf{I} & (\tilde{\Phi}_F^{\text{inc}})_{\text{wg1}}^+ (\tilde{\Phi}_F^{\text{ref}})_{\text{wg1}} \tilde{\mu}_{\text{wg1}}^{N_1} & \mathbf{0} & \mathbf{0} \\ -\tilde{C}_{11}\tilde{\mu}_{\text{wg1}}^{N_1} & \mathbf{I} & \mathbf{0} & -\tilde{C}_{12}\tilde{\mu}_{\text{wg2}}^{N_2} \\ \hline -\tilde{C}_{21}\tilde{\mu}_{\text{wg1}}^{N_1} & \mathbf{0} & \mathbf{I} & -\tilde{C}_{22}\tilde{\mu}_{\text{wg2}}^{N_2} \\ \mathbf{0} & \mathbf{0} & (\tilde{\Phi}_q^{\text{inc}})_{\text{wg2}}^+ (\tilde{\Phi}_q^{\text{ref}})_{\text{wg2}} \tilde{\mu}_{\text{wg2}}^{N_2} & \mathbf{I} \end{array} \right] \times \left[\begin{array}{cc|cc} \mathbf{I} & \mathbf{0} & \mathbf{0} & \mathbf{0} \\ \mathbf{0} & \tilde{\mu}_{\text{wg1}}^{-N_1} & \mathbf{0} & \mathbf{0} \\ \hline \mathbf{0} & \mathbf{0} & \tilde{\mu}_{\text{wg2}}^{-N_2} & \mathbf{0} \\ \mathbf{0} & \mathbf{0} & \mathbf{0} & \mathbf{I} \end{array} \right] \begin{pmatrix} \tilde{Q}_{\text{wg1}}^{\text{inc}(1)} \\ \tilde{Q}_{\text{wg1}}^{\text{ref}(1)} \\ \tilde{Q}_{\text{wg2}}^{\text{ref}(1)} \\ \tilde{Q}_{\text{wg2}}^{\text{inc}(1)} \end{pmatrix} = \begin{pmatrix} -(\tilde{\Phi}_F^{\text{inc}})_{\text{wg1}}^+ \mathbf{F}_0 \\ \mathbf{0} \\ \mathbf{0} \\ (\tilde{\Phi}_q^{\text{inc}})_{\text{wg2}}^+ \mathbf{q}_0 \end{pmatrix}. \quad (44)$$

Solving Eq. (44) provides the modal amplitudes $\{\tilde{Q}_{\text{wg1}}^{\text{inc}(1)}, \tilde{Q}_{\text{wg1}}^{\text{ref}(1)}\}$ and $\{\tilde{Q}_{\text{wg2}}^{\text{inc}(1)}, \tilde{Q}_{\text{wg2}}^{\text{ref}(1)}\}$, at the ends of waveguides 1 and 2 where forces and displacements are respectively prescribed. The spatial distribution of the modal amplitude along each waveguide is obtained by means of Eqs. (21) and (22). The spatial distribution of the kinematic variables (say displacements and forces) are finally provided by means of Eqs. (19) and (20).

4.3. Numerical results

4.3.1. Beam-like structure

We address the forced response of a straight clamped beam-like structure, with rectangular cross-section, whose free end is submitted to either axial or transverse loads. Here, the force field is assumed to be uniformly spread on the surface boundary. The material and geometric characteristics of the structure are: Young's modulus $E = 2 \times 10^{11} Pa$, density $\rho = 7800 kg.m^{-3}$, Poisson's ratio $\nu = 0.3$, loss factor $\eta = 0.01$, length $L = 2m$ and cross-section area $h_y \times h_z = 0.2m \times 0.3m$. The FE model of the global elastic system is depicted in Figure 2. It contains 21,000 DOFs and is composed of $N = 200$ identical substructures along the length, say the x -direction. Each substructure is meshed using 4×6 linear rectangular brick elements and exhibits a length $d = 0.01m$ (see Figure 2). This mesh is supposed to be fine enough to correctly capture the short wavelengths of the *significantly contributing* wave modes traveling along the x -direction [6], as well as the resulting wave shapes over the cross-section. The left and right boundaries of the substructure contains $n = 105$ DOFs providing that 105 incident and 105 reflected modes are obtained through the WFE eigenvalue problem (6). The forced responses of the global structure under either axial or transverse load (see Figure 2) are addressed on a frequency band $\mathcal{B}_f = [10Hz, 10^4Hz]$. Eq. (35) is computed for providing, by means of Eqs. (19) and (20), the WFE displacement solution. The wave basis $\{\tilde{\Phi}_j\}_j$ is supposed to include the modes which mostly contribute to the forced response of the structure. These relate particular "cross-section" shapes with both displacement and force components that can exhibit largely disparate spatial dynamics. The displacements components of several contributing wave shapes are depicted in Figure 3 at $7500Hz$. These refer to as the classic LF longitudinal,

flexural and shearing modes with a non-uniform spatial behavior ⁴, and MF higher order modes with an oscillating spatial dynamics for capturing the cross-section resonances.

Figure 2

Figure 3

The forced response of the global structure under axial load is computed first, when $m = 10$ and $m = 60$ wave modes are alternatively retained in $\{\tilde{\Phi}_j\}_j$. The longitudinal displacement of one corner of the excited cross-section is shown in Figure 4. Comparisons with a reference solution provided by the FE model of the global structure are also presented. The dimension of the wave-based matrix problem is $2m$, say 20 or 120, while the dimension of the full FE model is 21,000: as expected, the involved CPU times appear largely disparate, say several seconds for the wave approach against more than one hour for the standard FE approach. Regarding Figure 4, the WFE solutions with 10 modes correlate the first global vibrational modes of the structure while it poorly estimates the resonance levels at higher frequencies, especially the one occurring at $7500Hz$ (depicted by an arrow). This is explained as the wave basis is not rich enough for reflecting the non-uniform spatial dynamics occurring within the cross-section at such frequencies. Using a wave basis with an extended dimension — say $m = 60$ —, which contains additional high order modes, clearly solves this lack of convergence below $8000Hz$.

Figure 4

⁴It is worth emphasizing that the rigid body assumption for the cross-section breaks down at high frequencies.

Above $8000Hz$, the wave approach still suffers from a lack of convergence for predicting the resonance frequencies, whatever the size of the wave basis. This problem is solved when the theoretical correspondences among incident and reflected modes, provided by means of Eq. (13), are accounted for in the WFE formulation. Recall that these relationships have been formulated to circumvent numerical dispersion effects generated by the eigenvalue problem (6); they enforce the coherence between incident and reflected modes, in the sense that the equalities $\|(\tilde{\Phi}_{\mathbf{q}}^{\text{inc}})_j\| = \|(\tilde{\Phi}_{\mathbf{q}}^{\text{ref}})_j\|$ and $\|(\tilde{\Phi}_{\mathbf{F}}^{\text{inc}})_j\| = \|(\tilde{\Phi}_{\mathbf{F}}^{\text{ref}})_j\|$ are perfectly transcribed $\forall j$ (see Section 2.3). The relevance of the resulting wave-based problem is clearly established in Figure 5, compared to the FE solution.

Figure 5

The same strategy — involving the relationships (13) — is used to compute the forced response of the structure under transverse load, on the same frequency band \mathcal{B}_f . The transverse displacement provided by Eq. (35) is calculated using wave mode bases with different dimensions $m = 10$ and $m = 40$ (see Figure 6). It appears that the wave approach perfectly correlates the reference solution when $m = 40$. This clearly emphasizes the feature of the WFE method, in the sense that the forced response of straight structures can be correctly addressed using wave-based models of extremely small size (say $2m = 80$ in this case).

Figure 6

4.3.2. *Reissner-Mindlin plate*

We address the forced response of a square Reissner-Mindlin plate with one edge clamped into a support driven by a prescribed transverse displacement. The FE model of the problem is depicted in Figure 7, where \mathbf{q}_0 reflects the displacement of the support. The material and geometric characteristics of the structure are:

Young's modulus $E = 2 \times 10^{11} Pa$, density $\rho = 7800 kg.m^{-3}$, Poisson's ratio $\nu = 0.3$, loss factor $\eta = 0.01$, shear correction factor $\kappa = 5/6$, area $L_x \times L_y = 1m \times 1m$, thickness $h = 0.002m$. The global system is composed of $N = 40$ identical substructures along the x -direction. Each substructure has a length $d = 0.025m$ and is meshed using triangular Reissner-Mindlin elements with 6 nodes (see Figure 7). It contains the same number of DOFs, say $n = 83$, onto its left and right edges, while it contains $n_I = 161$ internal DOFs. The formulation of the symplectic matrix \mathbf{S} (see Eq. (3)), involved in the WFE eigenvalue problem, requires the dynamic stiffness operator of a typical substructure to be condensed onto its left and right boundaries [5]. This yields:

$$\mathbf{D}^* = \mathbf{D}_{BB} - \mathbf{D}_{BI}(\mathbf{D}_{II})^{-1}\mathbf{D}_{IB}, \quad (45)$$

where the subscript B denotes the DOFs contained onto the left and right boundaries, while the subscript I denotes the internal DOFs.

Figure 7

The forced response of the global structure is computed on a frequency band $\mathcal{B}_f = [10Hz, 2000Hz]$. Eq. (35) is computed for providing, by means of Eqs. (19) and (20), the WFE displacement solution. The coherence among incident and reflected modes is enforced through Eq. (13). The transverse displacement at the mid-side of the free edge, opposite to the support, is drawn in Figure 8. Comparisons with a reference solution provided by the FE model of the global structure are presented. The WFE solution is calculated using reduced wave bases of different dimensions, say $m = 10$, $m = 40$, $m = 60$ and $m = 80$. It is shown that the WFE formulation offers good convergence provided that it almost involves the full wave mode basis $\{\Phi_j\}_j$. This particularly means that the global structure reveals a complex behavior — particularly in the vicinity of the clamped edge and

corners where kinematic fields with local sharp gradients occur — which need to be spanned by highly oscillating cross-section wave shapes. Some of these shapes — these relate the transverse displacement components of the modes at $1500Hz$ — are drawn in Figure 9.

Figure 8

Figure 9

4.3.3. Two coupled beam-like structures

We address the forced response of two beam-like structures — namely waveguide 1 and waveguide 2 — with rectangular cross-sections, coupled through an elastic junction over one of their cross-section limits. Here, the elastic junction represents a quarter of torus. The finite element model of the coupled system is depicted in Figure 10. The other cross-section limits, for waveguide 2 and waveguide 1, are respectively clamped and submitted to a uniform transverse force field (in the z -direction) that reflects the vector \mathbf{F}_0 . The main axes of the two waveguides, say axes x_1 and x_2 , are perpendicular so that coupling among wave modes of different natures (say for instance, longitudinal, flexural, torsional) is likely to occur. The two waveguides, as well as the coupling junction, exhibit the same material characteristics: Young's modulus $E = 2 \times 10^{11} Pa$, density $\rho = 7800 kg.m^{-3}$, Poisson's ratio $\nu = 0.3$, loss factor $\eta = 0.01$. The two waveguides have the same cross-section area $h_y \times h_z = 0.2m \times 0.15m$, while their respective lengths are $L_1 = 2m$ and $L_2 = 1.5m$. The junction represents a quarter of torus with an internal radius of curvature $R_c = 0.05m$ and a cross-section similar to those of the connected waveguides. These are discretized with similar substructures of length $d = 0.01m$ (see Figure 10), so that waveguide 1 contains $N_1 = 200$ substructures and waveguide 2 contains $N_2 = 150$ substructures.

Figure 10

Each substructure is meshed using 4×3 linear rectangular brick elements, while $4 \times 3 \times 10$ linear brick elements are used for the discretization of the elastic junction. The mesh tying problem is illustrated in Figure 10 and reflects two substructures, used for wave mode description, coupled with the junction [5]. Here, the mesh compatibility across the coupling interfaces — namely Γ_1 (between the substructure 1 and the junction) and Γ_2 (between the substructure 2 and the junction) — is assumed, so that the coupling conditions are simply expressed as:

$$\mathbf{q}_{wg1}|_{\Gamma_1} = \mathbf{q}_c|_{\Gamma_1} \quad \text{and} \quad \mathbf{q}_{wg2}|_{\Gamma_2} = \mathbf{q}_c|_{\Gamma_2}, \quad (46)$$

$$\mathbf{F}_{wg1}|_{\Gamma_1} = -\mathbf{F}_c|_{\Gamma_1} \quad \text{and} \quad \mathbf{F}_{wg2}|_{\Gamma_2} = -\mathbf{F}_c|_{\Gamma_2}, \quad (47)$$

where subscript c refers to as the coupling junction. In this case, the diffusion matrix $\tilde{\mathbb{C}}$ (cf. Eq. (38)) is simply expressed as [5, 24]:

$$\tilde{\mathbb{C}} = - \left[\mathbb{K}^* \tilde{\Psi}_{\mathbf{q}}^{\text{ref}} + \tilde{\Psi}_{\mathbf{F}}^{\text{ref}} \right]^+ \left[\mathbb{K}^* \tilde{\Psi}_{\mathbf{q}}^{\text{inc}} + \tilde{\Psi}_{\mathbf{F}}^{\text{inc}} \right], \quad (48)$$

where \mathbb{K}^* stands for the dynamic stiffness matrix of the junction condensed onto Γ_1 and Γ_2 .

The forced response of the global structure is addressed using the WFE method. For this task, the modal amplitudes $\{\tilde{\mathbf{Q}}_{wg1}^{\text{inc}(1)}, \tilde{\mathbf{Q}}_{wg1}^{\text{ref}(1)}\}$ and $\{\tilde{\mathbf{Q}}_{wg2}^{\text{inc}(1)}, \tilde{\mathbf{Q}}_{wg2}^{\text{ref}(1)}\}$ are numerically calculated by means of Eq. (44). Again, the theoretical correspondences among incident and reflected modes, for each waveguide, are numerically imposed by means of Eq. (13). The WFE displacement solution for the two waveguides is obtained using Eqs. (19) and (20). The transverse displacement of one corner of the excited cross-section of waveguide 1 is computed on a frequency band $\mathcal{B}_f = [10Hz, 5000Hz]$ (see Figure 11). Comparisons with a reference solution provided by the FE model of the global structure are also presented. The wave-based problem is alternatively formulated from reduced bases containing $m = 10$

and $m = 40$ wave modes for each waveguide. Again, the convergence is achieved when a sufficient number — say $m = 40$ — of wave modes is accounted for. In this case, the selected wave modes constitute a complete family for spanning the behavior of each waveguide as well as the trace of the dynamic behavior of the junction onto the interfaces Γ_1 and Γ_2 [24].

Figure 11

4.3.4. Conclusions

The WFE formulation, based on the numerical problems (34) and (44), has been successfully used for computing the forced responses of a large variety of homogeneous systems, namely a clamped beam-like structure under axial or transverse load, a square Reissner-Mindlin plate under prescribed transverse displacement and a coupled system — say two waveguides coupled through an elastic junction — under transverse load. It has been shown that the WFE solutions successfully match the solutions provided by the standard FE method, that is when the global structure is discretized, provided that they are computed using wave bases of large enough size to capture the relative complexity of the cross-section spatial dynamics. Summarizing, the wave-based strategy offers the possibility to investigate the LF and MF behavior of structures using numerical models of small size. The feature of the WFE method is that the resulting CPU times appear considerably lowered compared to those involved by the standard FE method.

5. Regularization strategy

5.1. Motivation

The wave-based numerical problems (34) and (44) may be ill-posed when multi-layered systems are addressed. Such structures can reveal a multi-scale be-

havior over their cross-section in the sense that the layers can reveal strongly disparate wavelengths, e.g. for a sandwich beam constituted of a soft rubber core surrounded by two stiff steel skins (see Figure 12). Here, large ratios between the components of $\tilde{\Phi}_q$, as well as between the components of $\tilde{\Phi}_F$, are likely to occur. Another issue is the fact that wave mode shapes $\{\tilde{\Phi}_j\}_j$ can be extremely close to each other, though their respective wavenumbers can be largely disparate (see ref. [16, 25] for further explanations). As a consequence, the computations of the matrices $(\tilde{\Phi}_F^{\text{inc}})^+ \tilde{\Phi}_F^{\text{ref}}$ and $(\tilde{\Phi}_q^{\text{ref}})^+ \tilde{\Phi}_q^{\text{inc}}$ in Eqs. (34), as well as the computation of the matrices $(\tilde{\Phi}_F^{\text{inc}})_{\text{wg1}}^+ (\tilde{\Phi}_F^{\text{ref}})_{\text{wg1}}$ and $(\tilde{\Phi}_q^{\text{inc}})_{\text{wg2}}^+ (\tilde{\Phi}_q^{\text{ref}})_{\text{wg2}}$ in Eq. (44), can be prone to severe rounding errors.

To highlight this issue, let us address the forced response of the sandwich beam depicted in Figure 12. Here, the skins — namely layers 1 and 3 — have the same characteristics: height $h^1 = h^3 = 2 \times 10^{-3}m$, same width $50 \times 10^{-3}m$, Young's modulus $E^1 = E^3 = 2.1 \times 10^{11}Pa$, density $\rho^1 = \rho^3 = 7850kg/m^3$, Poisson's ratio $\nu^1 = \nu^3 = 0.3$. The core — namely layer 2 — exhibits the following characteristics: height $h^2 = 20 \times 10^{-3}m$, width $50 \times 10^{-3}m$, Young's modulus $E^2 = 1.5 \times 10^6Pa$, density $\rho^2 = 950kg/m^3$ and Poisson's ratio $\nu^2 = 0.48$. The global structure has a length $L = 0.4m$ and is assumed to be dissipative, in the sense that the three layers are assumed to have the same loss factor, say $\eta = 0.01$. The FE discretization of the global structure involves $N = 200$ identical multi-layered substructures connected along the x - axis. A typical multi-layered substructure is shown in Figure 12. It exhibits a length $d = 2 \times 10^{-3}m$ which is supposed to be small enough with regard to the wavelengths of the contributing wave modes, within the frequency band of interest. The three layers are meshed using linear rectangular brick elements: layers 1 and 3 (steel skins) are meshed with four elements while layer 2 (soft core) is meshed with sixteen elements. Within the WFE framework, this relatively coarse mesh should be appropriate to yield the

classic LF modes of the global system as well as several MF modes, for which the core cross-section reveals local dynamics. The spatial distributions of several wave mode shapes obtained when computing the eigenvalue problem (6) are depicted in Figure 13.

Figure 12

Figure 13

The forced response of the sandwich structure clamped at the right end, over the whole cross-section, and excited at the left end, over the bottom skin cross-section, is calculated on a frequency band $\mathcal{B}_f = [100Hz, 1500Hz]$. Longitudinal and transverse loads, as depicted in Figure 12, are individually studied. These loads numerically describe surface force fields which are uniformly spread on the bottom skin cross-section. The longitudinal and transverse displacements of a corner of the excited bottom skin cross-section, provided by the wave-based problem (34) when longitudinal and transverse loads are respectively applied, are drawn in Figures 14 and 15. Comparisons with a reference solution provided by the full FE model of the sandwich structure, with 21,000 DOFs, are also presented. For each type of excitation, the WFE solutions are calculated using wave bases of different dimensions, say $m = 10$, $m = 30$, $m = 50$ and $m = 70$. With $m = 10$, the WFE method clearly reveals a lack of convergence as the frequency increases, whatever the type of excitations. This issue has been discussed in depth in ref. [16, 25] and can be explained as the wave modes reveal changes of natures within \mathcal{B}_f , providing that the classic wave motions (longitudinal and flexural among others) are obliterated in the WFE formulation. This can be solved using wave bases with extended dimensions — say $m = 30$, $m = 50$ and $m = 70$ — so as to reflect these classic motions during and after the wave mode conversion process.

Figure 14

Figure 15

Another problem is that the WFE solutions may reveal local discontinuities as well as spurious resonances/oscillations within \mathcal{B}_f (cf. the WFE solutions computed with $m = 30$ and $m = 50$). These numerical instabilities and pollution effects introduce approximatively the same amount of errors when $m = 30$ and $m = 50$, although their frequency descriptions can strongly differ. In other words, the wave-based problem (34) appears sensitive to the dimension of the wave basis while the way of increasing its size does not significantly improve the convergence of the formalism, contrary to what was observed for homogeneous systems (see Section 4.3). Numerical instabilities finally disappear when $m = 70$: in this case, the WFE solution perfectly correlates, within \mathcal{B}_f , the reference FE solution when longitudinal excitation is considered, while it still suffers from a lack of convergence to address the local resonances above $1000Hz$ when transversal excitation is concerned.

Summarizing, the wave-based problem reveals poor consistency for describing the behavior of the sandwich structure, as it introduces numerical instabilities and pollution effects. Numerical instabilities can be removed away if wave bases of extremely large dimensions are accounted for in the formalism, while it appears not clear whether increasing the size of the basis completely provides the local resonances of the structure over the entire frequency band \mathcal{B}_f . The drawback of the formulation — say numerical instabilities and pollution effects — results from the computations of $(\tilde{\Phi}_F^{\text{inc}})^+ \tilde{\Phi}_F^{\text{ref}}$ and $(\tilde{\Phi}_q^{\text{ref}})^+ \tilde{\Phi}_q^{\text{inc}}$ in Eq. (34), as underlined above. A regularization strategy is proposed hereafter to treat these issues.

5.2. Wave mode expansion

The framework of the regularization strategy is to use an alternative family of wave mode shapes — namely $\{\tilde{\Phi}_j^{\text{inc}}\}_{j=1,\dots,m} \cup \{\tilde{\Upsilon}_j^{\text{ref}}\}_{j=1,\dots,m}$ — as representation basis. The resulting wave mode expansion is

$$\mathbf{u}_L^{(k)} = \tilde{\Phi}^{\text{inc}} \tilde{\mathbf{Q}}^{\text{inc}(k)} + \tilde{\Upsilon}^{\text{ref}} \tilde{\mathbf{Q}}^{\text{ref}(k)} \quad k = 1, \dots, N, \quad (49)$$

$$\mathbf{u}_R^{(k)} = \tilde{\Phi}^{\text{inc}} \tilde{\mathbf{Q}}^{\text{inc}(k+1)} + \tilde{\Upsilon}^{\text{ref}} \tilde{\mathbf{Q}}^{\text{ref}(k+1)} \quad k = 1, \dots, N, \quad (50)$$

where $\tilde{\Upsilon}^{\text{ref}}$ refers to as the matrix form of $\{\tilde{\Upsilon}_j^{\text{ref}}\}_{j=1,\dots,m}$ and is defined such that

$$\tilde{\Upsilon}^{\text{ref}} = \begin{bmatrix} \tilde{\Upsilon}_q^{\text{ref}} \\ \tilde{\Upsilon}_F^{\text{ref}} \end{bmatrix} = \begin{bmatrix} \tilde{\Phi}_q^{\text{inc}} \\ -\tilde{\Phi}_F^{\text{inc}} \end{bmatrix}. \quad (51)$$

The matrix $\tilde{\Upsilon}^{\text{ref}}$ is directly computed using the incident mode shapes $\tilde{\Phi}^{\text{inc}}$. The shapes $\{\tilde{\Upsilon}_j^{\text{ref}}\}_j$ play the role of reflected modes and appear strongly correlated to the shapes of the incident modes as $\|(\tilde{\Phi}_q^{\text{inc}})_j\| = \|(\tilde{\Upsilon}_q^{\text{ref}})_j\|$ and $\|(\tilde{\Phi}_F^{\text{inc}})_j\| = \|(\tilde{\Upsilon}_F^{\text{ref}})_j\| \forall j$. The choice of this alternative basis lies in the fact that the computation of the matrices $(\tilde{\Phi}_F^{\text{inc}})^+ \tilde{\Phi}_F^{\text{ref}}$ and $(\tilde{\Phi}_q^{\text{ref}})^+ \tilde{\Phi}_q^{\text{inc}}$ in Eq. (34) can be circumvented since the following substitutions operate:

$$(\tilde{\Phi}_F^{\text{inc}})^+ \tilde{\Phi}_F^{\text{ref}} \rightarrow (\tilde{\Phi}_F^{\text{inc}})^+ \tilde{\Upsilon}_F^{\text{ref}} = -\mathbf{I}, \quad (52)$$

$$(\tilde{\Phi}_q^{\text{ref}})^+ \tilde{\Phi}_q^{\text{inc}} \rightarrow (\tilde{\Upsilon}_q^{\text{ref}})^+ \tilde{\Phi}_q^{\text{inc}} = \mathbf{I}. \quad (53)$$

It is worth noting that the definitions (51) are quite natural when incident and reflected wave shapes represent longitudinal wave motion⁵. The validity of this alternative wave mode expansion is investigated hereafter:

Proposition 4. Let us assume that the reduced basis $\{\tilde{\Phi}_j^{\text{inc}}\}_j \cup \{\tilde{\Upsilon}_j^{\text{ref}}\}_j$ is composed of wave modes which effectively contribute to the forced response of

⁵This is readily verified for LF analytic solutions [26].

the structure, depending on the manner by which the excitation sources are applied. The governing equations (21) and (22) can be applied provided that the following conditions are verified:

- (i) Each vector $\tilde{\Upsilon}_j^{\text{ref}}$ is a linear combination of the wave modes $\{\tilde{\Phi}_k^{\text{ref}}\}_{k=1,\dots,m}$, i.e. $\tilde{\Upsilon}^{\text{ref}} = \tilde{\Phi}^{\text{ref}} \alpha$, where α is a $(m \times m)$ matrix;
- (ii) α is invertible;
- (iii) $\tilde{\mu}$ and α almost commute.

Proof. Inserting Eqs. (49) and (50) into $\mathbf{u}_r^{(k-1)} = \mathbf{S}^{k-1} \mathbf{u}_L^1$ — provided by the recurrence equation (5) and the coupling conditions (4) —, and accounting that $\mathbf{S}^{k-1} \tilde{\Phi}^{\text{inc}} = \tilde{\Phi}^{\text{inc}} \tilde{\mu}^{k-1}$, leads to

$$\tilde{\Phi}^{\text{inc}} \tilde{\mathbf{Q}}^{\text{inc}(k)} + \tilde{\Upsilon}^{\text{ref}} \tilde{\mathbf{Q}}^{\text{ref}(k)} = \tilde{\Phi}^{\text{inc}} \tilde{\mu}^{k-1} \tilde{\mathbf{Q}}^{\text{inc}(1)} + \mathbf{S}^{k-1} \tilde{\Upsilon}^{\text{ref}} \tilde{\mathbf{Q}}^{\text{ref}(1)}. \quad (54)$$

According to (i), this results in

$$\tilde{\Phi}^{\text{inc}} \tilde{\mathbf{Q}}^{\text{inc}(k)} + \tilde{\Phi}^{\text{ref}} \alpha \tilde{\mathbf{Q}}^{\text{ref}(k)} = \tilde{\Phi}^{\text{inc}} \tilde{\mu}^{k-1} \tilde{\mathbf{Q}}^{\text{inc}(1)} + \mathbf{S}^{k-1} \tilde{\Phi}^{\text{ref}} \alpha \tilde{\mathbf{Q}}^{\text{ref}(1)}. \quad (55)$$

Given that $\mathbf{S}^{k-1} \tilde{\Phi}^{\text{ref}} = \tilde{\Phi}^{\text{ref}} \tilde{\mu}^{-(k-1)}$, Eq. (55) gives

$$\tilde{\Phi}^{\text{inc}} \tilde{\mathbf{Q}}^{\text{inc}(k)} + \tilde{\Phi}^{\text{ref}} \alpha \tilde{\mathbf{Q}}^{\text{ref}(k)} = \tilde{\Phi}^{\text{inc}} \tilde{\mu}^{k-1} \tilde{\mathbf{Q}}^{\text{inc}(1)} + \tilde{\Phi}^{\text{ref}} \tilde{\mu}^{-(k-1)} \alpha \tilde{\mathbf{Q}}^{\text{ref}(1)}. \quad (56)$$

Left multiplying Eq. (56) by $(\tilde{\Phi}^{\text{ref}})^T \mathbf{J}$ and accounting for the symplectic orthogonality property (9) clearly leads to $\tilde{\mathbf{Q}}^{\text{inc}(k)} = \tilde{\mu}^{k-1} \tilde{\mathbf{Q}}^{\text{inc}(1)} \forall k$. On the other hand, left multiplying Eq. (56) by $(\tilde{\Phi}^{\text{inc}})^T \mathbf{J}$ and accounting for Eq. (9) gives

$$(\tilde{\Phi}^{\text{inc}})^T \mathbf{J} \tilde{\Phi}^{\text{ref}} \alpha \tilde{\mathbf{Q}}^{\text{ref}(k)} = (\tilde{\Phi}^{\text{inc}})^T \mathbf{J} \tilde{\Phi}^{\text{ref}} \tilde{\mu}^{-(k-1)} \alpha \tilde{\mathbf{Q}}^{\text{ref}(1)}, \quad (57)$$

which leads to

$$\alpha \tilde{\mathbf{Q}}^{\text{ref}(k)} = \tilde{\mu}^{-(k-1)} \alpha \tilde{\mathbf{Q}}^{\text{ref}(1)}, \quad (58)$$

as the matrix $(\tilde{\Phi}^{\text{inc}})^T \mathbf{J} \tilde{\Phi}^{\text{ref}}$ is diagonal and supposed to be invertible. Using (ii), Eq. (58) can be rewritten as

$$\tilde{\mathbf{Q}}^{\text{ref}(k)} = \alpha^{-1} \tilde{\mu}^{-(k-1)} \alpha \tilde{\mathbf{Q}}^{\text{ref}(1)}. \quad (59)$$

Accounting for (iii) — providing that $\tilde{\mu} \alpha \approx \alpha \tilde{\mu}$ ⁶, that is to say $\tilde{\mu}^{-(k-1)} \alpha \approx \alpha \tilde{\mu}^{-(k-1)} \forall k$ — into Eq. (59) finally results in $\tilde{\mathbf{Q}}^{\text{ref}(k)} = \tilde{\mu}^{-(k-1)} \tilde{\mathbf{Q}}^{\text{ref}(1)} \forall k$.

□

Remark 6. It is not straightforward whether matrices $\tilde{\mu}$ and α almost commute since α is not diagonal in general. This is explained as the construction of the wave modes $\{\tilde{\Upsilon}_j^{\text{ref}}\}_j$ and $\{\tilde{\Phi}_j^{\text{ref}}\}_j$ — provided by Eqs. (51) and (13), respectively — can be quite different with regard to the symmetry transformation matrix \mathcal{R} , when the rotation of the cross-section induces non-negligible values within the components of $\{\tilde{\Phi}_j^{\text{inc}}\}_j$. For a pure transverse excitation involving flexural wave motions as contributing modes, these values can be lowered provided that the cross-section reveals a sufficiently small height in the direction of the load. For a pure longitudinal excitation, there is no such limitation as the contributing modes $\{\tilde{\Upsilon}_j^{\text{ref}}\}_j$ and $\{\tilde{\Phi}_j^{\text{ref}}\}_j$ are longitudinal i.e. they are identically formulated by means of Eqs. (51) and (13).

Remark 7. It is clear that the governing equations (21) and (22) can be stated even though the reduced basis $\{\tilde{\Phi}_j^{\text{inc}}\}_j \cup \{\tilde{\Upsilon}_j^{\text{ref}}\}_j$ includes weakly contributing modes⁷, in the sense that their influence is negligible.

⁶A more rigorous definition is to say that $\|\tilde{\mu} \alpha - \alpha \tilde{\mu}\| \leq \epsilon$ where ϵ is a second order of $\min\{\|\tilde{\mu} \alpha\|, \|\alpha \tilde{\mu}\|\}$ (see ref. [27] for further discussions).

⁷Recall that the selection of the reduced basis is rather empirical and based on the way they are or become propagating behind a certain limiting frequency, whatever the excitation source.

5.3. Boundary value problem

Using Eqs. (49), (50) and (51), the boundary conditions (27) and (28) of a single waveguide, whose left and right boundaries are respectively submitted to prescribed forces and prescribed displacements, write:

$$\tilde{\Phi}_F^{\text{inc}} \tilde{\mathbf{Q}}^{\text{inc}(1)} - \tilde{\Phi}_F^{\text{inc}} \tilde{\mathbf{Q}}^{\text{ref}(1)} = -\mathbf{F}_0, \quad (60)$$

$$\tilde{\Phi}_q^{\text{inc}} \tilde{\mathbf{Q}}^{\text{inc}(N+1)} + \tilde{\Phi}_q^{\text{inc}} \tilde{\mathbf{Q}}^{\text{ref}(N+1)} = \mathbf{q}_0. \quad (61)$$

Also, using the governing equations (21) and (22) results in

$$\tilde{\Phi}_F^{\text{inc}} \tilde{\mathbf{Q}}^{\text{inc}(1)} - \tilde{\Phi}_F^{\text{inc}} \tilde{\mathbf{Q}}^{\text{ref}(1)} = -\mathbf{F}_0, \quad (62)$$

$$\tilde{\Phi}_q^{\text{inc}} \tilde{\mu}^N \tilde{\mathbf{Q}}^{\text{inc}(1)} + \tilde{\Phi}_q^{\text{inc}} \tilde{\mu}^{-N} \tilde{\mathbf{Q}}^{\text{ref}(1)} = \mathbf{q}_0, \quad (63)$$

which, in matrix form, gives

$$\begin{bmatrix} \mathbf{I} & -\tilde{\mu}^N \\ \tilde{\mu}^N & \mathbf{I} \end{bmatrix} \begin{bmatrix} \mathbf{I} & \mathbf{0} \\ \mathbf{0} & \tilde{\mu}^{-N} \end{bmatrix} \begin{pmatrix} \tilde{\mathbf{Q}}^{\text{inc}(1)} \\ \tilde{\mathbf{Q}}^{\text{ref}(1)} \end{pmatrix} = \begin{pmatrix} -(\tilde{\Phi}_F^{\text{inc}})^+ \mathbf{F}_0 \\ (\tilde{\Phi}_q^{\text{inc}})^+ \mathbf{q}_0 \end{pmatrix}, \quad (64)$$

where appropriate scalings have been used (cf. Section 4.1). The system (64) involves matrices whose inverses can be computed without difficulties. The drawbacks of the classic WFE problem (34), caused by the computations of $(\tilde{\Phi}_F^{\text{inc}})^+ \tilde{\Phi}_F^{\text{ref}}$ and $(\tilde{\Phi}_q^{\text{ref}})^+ \tilde{\Phi}_q^{\text{inc}}$, are circumvented through the regularization strategy (see Eqs. (52) and (53)). Solving the system (64) finally gives

$$\begin{pmatrix} \tilde{\mathbf{Q}}^{\text{inc}(1)} \\ \tilde{\mathbf{Q}}^{\text{ref}(1)} \end{pmatrix} = \begin{bmatrix} \mathbf{I} & \mathbf{0} \\ \mathbf{0} & \tilde{\mu}^N \end{bmatrix} \begin{bmatrix} \mathbf{I} & -\tilde{\mu}^N \\ \tilde{\mu}^N & \mathbf{I} \end{bmatrix}^{-1} \begin{pmatrix} -(\tilde{\Phi}_F^{\text{inc}})^+ \mathbf{F}_0 \\ (\tilde{\Phi}_q^{\text{inc}})^+ \mathbf{q}_0 \end{pmatrix}, \quad (65)$$

where $\{\tilde{\mathbf{Q}}^{\text{inc}(1)}, \tilde{\mathbf{Q}}^{\text{ref}(1)}\}$ represent the modal amplitudes for the left cross-section limit of the waveguide, where forces are prescribed. The spatial distribution of the modal amplitude is obtained by means of Eqs. (21) and (22). The spatial distribution of the kinematic variables (say displacements and forces) finally result from

Eqs. (19) and (20).

Remark 8. The regularized wave-based boundary value problem can suffer from a lack of convergence for predicting the antiresonances, i.e. for frequencies where two dual incident and reflected wave modes exhibit equal magnitudes and opposite phases so that their contributions cancel each other. This is explained as the symmetry property of these modes (see Eq. (13)) is not well transcribed through the regularized strategy (for flexural wave motions especially).

The regularization strategy based on Eqs. (49) and (50) can be used for addressing the forced response of coupled systems. The resulting problem, for two waveguides coupled through an elastic junction, is simply formulated as

$$\begin{aligned}
& \left[\begin{array}{cc|cc} \mathbf{I} & -\tilde{\boldsymbol{\mu}}_{\text{wg1}}^{N_1} & \mathbf{0} & \mathbf{0} \\ -\tilde{\mathbf{C}}_{11}\tilde{\boldsymbol{\mu}}_{\text{wg1}}^{N_1} & \mathbf{I} & \mathbf{0} & -\tilde{\mathbf{C}}_{12}\tilde{\boldsymbol{\mu}}_{\text{wg2}}^{N_2} \\ \hline -\tilde{\mathbf{C}}_{21}\tilde{\boldsymbol{\mu}}_{\text{wg1}}^{N_1} & \mathbf{0} & \mathbf{I} & -\tilde{\mathbf{C}}_{22}\tilde{\boldsymbol{\mu}}_{\text{wg2}}^{N_2} \\ \mathbf{0} & \mathbf{0} & \tilde{\boldsymbol{\mu}}_{\text{wg2}}^{N_2} & \mathbf{I} \end{array} \right] \left[\begin{array}{cc|cc} \mathbf{I} & \mathbf{0} & \mathbf{0} & \mathbf{0} \\ \mathbf{0} & \tilde{\boldsymbol{\mu}}_{\text{wg1}}^{-N_1} & \mathbf{0} & \mathbf{0} \\ \hline \mathbf{0} & \mathbf{0} & \tilde{\boldsymbol{\mu}}_{\text{wg2}}^{-N_2} & \mathbf{0} \\ \mathbf{0} & \mathbf{0} & \mathbf{0} & \mathbf{I} \end{array} \right] \begin{pmatrix} \tilde{\mathbf{Q}}_{\text{wg1}}^{\text{inc}(1)} \\ \tilde{\mathbf{Q}}_{\text{wg1}}^{\text{ref}(1)} \\ \hline \tilde{\mathbf{Q}}_{\text{wg2}}^{\text{ref}(1)} \\ \tilde{\mathbf{Q}}_{\text{wg2}}^{\text{inc}(1)} \end{pmatrix} \\
& = \begin{pmatrix} -(\tilde{\boldsymbol{\Phi}}_{\text{F}}^{\text{inc}})_{\text{wg1}}^+ \mathbf{F}_0 \\ \mathbf{0} \\ \hline \mathbf{0} \\ (\tilde{\boldsymbol{\Phi}}_{\text{q}}^{\text{inc}})_{\text{wg2}}^+ \mathbf{q}_0 \end{pmatrix}, \tag{66}
\end{aligned}$$

where the computations of the matrices $(\tilde{\boldsymbol{\Phi}}_{\text{F}}^{\text{inc}})_{\text{wg1}}^+(\tilde{\boldsymbol{\Phi}}_{\text{F}}^{\text{ref}})_{\text{wg1}}$ and $(\tilde{\boldsymbol{\Phi}}_{\text{q}}^{\text{inc}})_{\text{wg2}}^+(\tilde{\boldsymbol{\Phi}}_{\text{q}}^{\text{ref}})_{\text{wg2}}$ (see the original problem (44)) are not required.

5.4. Numerical validation

5.4.1. Sandwich structure

We address the forced response of the sandwich structure previously depicted in Section 5.1 (see Figure 12), using the regularization strategy based on the wave

mode expansion (49) and (50). This strategy is used for calculating the displacement solution at a corner of the left cross-section limit, when the wave mode amplitudes are computed by means of Eq. (65). The frequency response of the structure under longitudinal and transverse loads are respectively drawn in Figures 16 and 17.

Figure 16

Figure 17

The resonances of the structures are quite well transcribed by the regularized wave-based problem. The relevance of the formalism for capturing the vibratory levels of the transversally excited structure over the entire frequency band is clearly established compared to the classic WFE method, despite some drawbacks for predicting the antiresonances (cf. Remark 8). The accuracy of the regularized formalism is reached when only a small number of wave modes are retained in the representation basis. The drawbacks of the classic WFE formulation — say, numerical instabilities and pollution effects above $500Hz$ (see Figure 15) — have been circumvented through the regularization strategy, as expected. Regarding the frequency response of the longitudinally excited structure, it can be emphasized however that the formalism suffer from pollution effects at low frequency (this is particularly verified when $m = 70$), as the dimension of the wave basis can exceed the vibration scale of the global cross-section [16]. In this sense, linear dependency among modes are favored and badly conditioned problems are likely to occur. However, these are not restrictive for the formulation and can easily be removed away provided that the frequency is not too close to zero, with regard to the fundamental resonance of the skins.

The relevance of the wave-based numerical problem (65) for predicting the behavior of the transversally excited structure can be justified in the present ex-

ample as the heights of the skin cross-sections, in the direction of the load, are small enough so that the rotations of these cross-sections are supposed to induce negligible values within the displacement and force components of $\{\tilde{\Phi}_j^{\text{inc}}\}_j$ (see Remark 6). Within these assumptions, the regularization strategy can be applied in theory to a large class of problems. As an example, the problem of determining the vibratory behavior of a Reissner-Mindlin plate is investigated hereafter.

5.4.2. Reissner-Mindlin plate

We address the frequency response of the Reissner-Mindlin plate previously depicted in Section 4.3.2 (see Figure 7). The solutions provided by the regularized wave-based problem are shown in Figure 18. The main resonances of the structure are correctly transcribed through the formalism, as expected. As was previously observed for the case of the sandwich structure, the accuracy of the regularized formalism is quickly raised for providing these resonances over the entire frequency band, i.e. when the size of the wave basis contains a small number of modes only (say $m = 40$). This seems to constitute an interesting feature of the regularized strategy compared to the classic WFE method (see Figure 8). This might be explained given that the contribution of high order MF modes does not appear lowered in the calculation of the regularized solution (65), contrary to what is simulated within the WFE framework when computing $(\tilde{\Phi}_F^{\text{inc}})^+ \tilde{\Phi}_F^{\text{ref}} \tilde{\mu}^N$ and $(\tilde{\Phi}_q^{\text{ref}})^+ \tilde{\Phi}_q^{\text{inc}} \tilde{\mu}^N$ in Eq. (35) (see Section 4.1).

Figure 18

5.4.3. Conclusions

The regularization strategy provided by the wave mode expansion (49) or (50) has been successfully used for describing the vibratory levels of a one-end-clamped sandwich structure and a one-edge-clamped Reissner-Mindlin plate. The strategy

exhibits two main features compared to the classic WFE formulation:

- It enables to circumvent numerical instabilities and pollution effects when multi-layered systems are addressed;
- The convergence of the resulting boundary value problem is quickly raised when the wave basis contains a small number of modes.

6. Concluding remarks

The low- and mid-frequency forced response of straight structures has been addressed using the WFE method. In this framework, the kinematic fields are expanded onto one-dimensional traveling wave modes, whose computation requires the finite element model of a typical substructure. Depending on the degree of complexity which is required for the spatial response, the mesh density of the substructure can be modified so as to enrich the wave basis with highly oscillating cross-section shapes. The WFE formulation has been investigated for addressing the Neumann-to-Dirichlet problem. The resulting matrix form has been adapted using appropriate scalings to circumvent poor conditioned problems, as the ratios between the wave force and wave displacement components can reach extremely large values. The formalism has been successfully validated for addressing the forced responses of a beam-like structure and a Reissner-Mindlin plate, as well as the forced response of two waveguides transversally coupled through an elastic junction. On the other hand, it has been emphasized that the WFE formulation can suffer from numerical instabilities and pollution effects when multi-layered systems are dealt with. The drawback of the method is that the wave components can be largely disparate over the global cross-section, providing that the resulting wave-based matrix problem can be ill-posed. A regularization strategy has been

proposed to solve this issue. It involves an alternative wave expansion by which reflected and incident modes are simply linked in a way similar to what is analytically stated for the plane longitudinal wave motion. More generally, it has been emphasized that the formalism can be applied to any transversally excited structures provided that the height of their cross-sections, in the direction of the load, is sufficiently small. The relevance of the regularization strategy has been established for predicting the vibratory levels of a sandwich beam under longitudinal and transverse loads, as well as a Reissner-Mindlin plate under transverse loads.

References

- [1] R. Ohayon, C. Soize, *Structural Acoustics and Vibration*, Academic Press, San Diego, 1998.
- [2] D. J. Mead, A general theory of harmonic wave propagation in linear periodic systems with multiple coupling, *Journal of Sound and Vibration* 27 (2) (1973) 235–260.
- [3] W. X. Zhong, F. W. Williams, On the direct solution of wave propagation for repetitive structures, *Journal of Sound and Vibration* 181 (3) (1995) 485–501.
- [4] O. C. Zienkiewicz, R. L. Taylor, *The Finite Element Method* (first volume), Butterworth-Heinemann, fifth edition, Oxford, 2000.
- [5] J.-M. Mencik, M. N. Ichchou, Multi-mode propagation and diffusion in structures through finite elements, *European Journal of Mechanics - A/Solids* 24 (5) (2005) 877–898.
- [6] J.-M. Mencik, M. N. Ichchou, Wave finite elements in guided elastodynamics with internal fluid, *International Journal of Solids and Structures* 44 (2007) 2148–2167.
- [7] E. Manconi, B. Mace, R. Gaziera, Wave finite element analysis of fluid-filled pipes, *Proceedings of NOVEM 2009 “Noise and Vibration: Emerging Methods”*, Oxford, UK.
- [8] B. Mace, D. Duhamel, M. J. Brennan, L. Hinke, Finite element prediction of wave motion in structural waveguides, *Journal of the Acoustical Society of America* 117 (2005) 2835.

- [9] Y. Waki, B. Mace, M. Brennan, Free and forced vibrations of a tyre using a wave/finite element approach, *Journal of Sound and Vibration* 323 (3-5) (2009) 737–756.
- [10] D. Duhamel, B. R. Mace, M. J. Brennan, Finite element analysis of the vibrations of waveguides and periodic structures, *Journal of Sound and Vibration* 294 (2006) 205–220.
- [11] Y. Waki, B. Mace, M. Brennan, Numerical issues concerning the wave and finite element method for free and forced vibrations of waveguides, *Journal of Sound and Vibration* 327 (1-2) (2009) 92–108.
- [12] Y. Yong, Y. K. Lin, Propagation of decaying waves in periodic and piecewise periodic structures of finite length, *Journal of Sound and Vibration* 129 (2) (1989) 99–118.
- [13] A. H. von Flotow, Disturbance propagation in structural networks, *Journal of Sound and Vibration* 106 (3) (1986) 433–450.
- [14] C. Wilcox, Theory of Bloch waves, *Journal d’Analyse Mathématique* 33.
- [15] G. J. Golub, C. F. V. Loan, *Matrix Computations*, The Johns Hopkins University Press, Baltimore and London, 1996.
- [16] J.-M. Mencik, M. N. Ichchou, A substructuring technique for finite element wave propagation in multi-layered systems, *Computer Methods in Applied Mechanics and Engineering* 197 (6-8) (2008) 505–523.
- [17] Y. Waki, On the applicability of finite element analysis to wave motion in one-dimensional waveguides, Ph. D. Thesis: University of Southampton (UK), Institute of Sound and Vibration Research.

- [18] N. G. Stephen, P. J. Wang, On transfer matrix eigenanalysis of pin-jointed frameworks, *Computers and Structures* 78 (2000) 603–615.
- [19] C. R. Fuller, F. J. Fahy, Characteristics of wave propagation and energy distributions in cylindrical elastic shells filled with fluid, *Journal of Sound and Vibration* 81 (4) (1982) 501–518.
- [20] G. J. Golub, J. H. Wilkinson, Ill-conditioned eigensystems and the computation of the Jordan canonical form, *SIAM Review* 18 (4) (1976) 578–619.
- [21] W. Yao, W. Zhong, C. W. Lim, *Symplectic Elasticity*, World Scientific Publishing, Singapore, 2009.
- [22] L. Gry, C. Gontier, Dynamic modelling of railway track: a periodic model based on a generalized beam formulation, *Journal of Sound and Vibration* 199 (4) (1997) 531–558.
- [23] J.-M. Mencik, M. N. Ichchou, L. Jézéquel, Propagation multimodale dans les systèmes périodiques couplés (in French), *Revue Européenne de Mécanique Numérique* 15 (1-3) (2006) 293–306.
- [24] M. N. Ichchou, J.-M. Mencik, W. J. Zhou, Wave finite elements for low and mid-frequency description of coupled structures with damage, *Computer Methods in Applied Mechanics and Engineering* 198 (15-16) (2009) 1311–1326.
- [25] J.-M. Mencik, On the forced response of multi-layered systems using the modified wave finite element method, *Proceedings of the Ninth International Conference on Computational Structures Technology*, Athens, Greece.
- [26] K. G. Graff, *Wave Motion in Elastic Solids*, Oxford University Press, London, 1991.

- [27] C. A. J. Luxemburg, R. F. Taylor, Almost commuting matrices are near commuting matrices, *Indagationes Mathematicae (Proceedings)* 73 (1970) 96–98.

List of Figures

1	Illustration of incident and reflected waves; FE model of a typical sub-structure.	47
2	FE model of a clamped beam-like structure under longitudinal (a) or transverse (b) load; FE model of a typical substructure (c).	48
3	Spatial representation of several “cross-section” wave mode shapes for the beam-like structure depicted in Figure 2, at $7500Hz$: (a) longitudinal mode; (b) flexural mode; (c) shearing mode; (d-i) MF modes.	49
4	Frequency response of the clamped beam-like structure depicted in Figure 2, under longitudinal load: (—) solutions provided by FE; (\cdots) solutions provided by WFE with 10 modes (a) and 60 modes (b).	50
5	Frequency response of the clamped beam-like structure depicted in Figure 2, under longitudinal load: (—) solutions provided by FE; (\cdots) solutions provided by WFE — based on Eq. (13) — with 10 modes (a) and 60 modes (b).	51
6	Frequency response of the clamped beam-like structure depicted in Figure 2, under transverse load: (—) solutions provided by FE; (\cdots) solutions provided by WFE — based on Eq. (13) — with 10 modes (a) and 40 modes (b).	52
7	FE model of a Reissner-Mindlin plate with on edge clamped into a support with prescribed displacement (a); FE model of a typical substructure (b).	53
8	Frequency response of the Reissner-Mindlin plate depicted in Figure 7: (—) solutions provided by FE; (\cdots) solutions provided by WFE with 10 modes (a), 40 modes (b), 60 modes (c) and 80 modes (d).	54

9	Spatial representation of several “cross-section” wave mode shapes for the Reissner-Mindlin plate depicted in Figure 7, at $1500Hz$: symmetric flexural LF and MF modes.	55
10	FE model of two waveguides coupled through an elastic junction (a); FE model of the underlying wave-based model, based on two coupled substructures (b).	56
11	Frequency response of the coupled system depicted in Figure 10: (—) solutions provided by FE; (\cdots) solutions provided by WFE with 10 modes (a) and 40 modes (b).	57
12	FE model of a sandwich beam under longitudinal (a) or transverse (b) load; FE model of a typical substructure (c).	58
13	Spatial representation of several “cross-section” wave mode shapes for the sandwich structure depicted in Figure 12, at $1000Hz$: (a) longitudinal mode; (b) shearing mode; (c) flexural mode; (d-i) MF modes.	59
14	Frequency response of the sandwich structure depicted in Figure 12, under longitudinal load: (—) solutions provided by FE; (\cdots) solutions provided by WFE with 10 modes (a), 30 modes (b), 50 modes (c) and 70 modes (d).	60
15	Frequency response of the sandwich structure depicted in Figure 12, under transverse load: (—) solutions provided by FE; (\cdots) solutions provided by WFE with 10 modes (a), 30 modes (b), 50 modes (c) and 70 modes (d).	61
16	Frequency response of the sandwich structure depicted in Figure 12, under longitudinal load: (—) solutions provided by FE; (\cdots) solutions provided by regularized WFE with 10 modes (a), 30 modes (b), 50 modes (c) and 70 modes (d).	62

17	Frequency response of the sandwich structure depicted in Figure 12, under transverse load: (—) solutions provided by FE; (···) solutions provided by regularized WFE with 10 modes (a), 30 modes (b), 50 modes (c) and 70 modes (d).	63
18	Frequency response of the Reissner-Mindlin plate depicted in Figure 7: (—) solutions provided by FE; (···) solutions provided by regularized WFE with 10 modes (a), 40 modes (b), 60 modes (c) and 80 modes (d). .	64

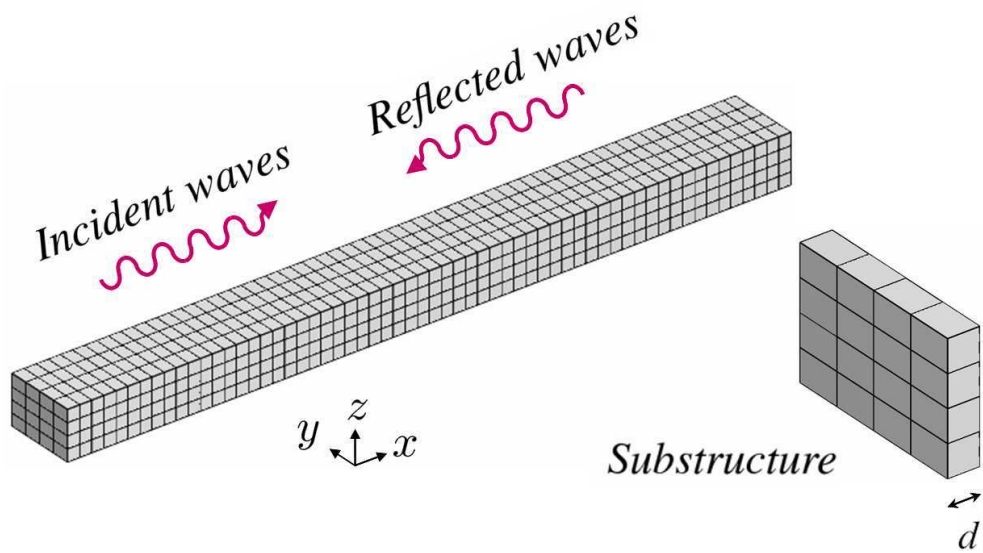


Figure 1: Illustration of incident and reflected waves; FE model of a typical substructure.

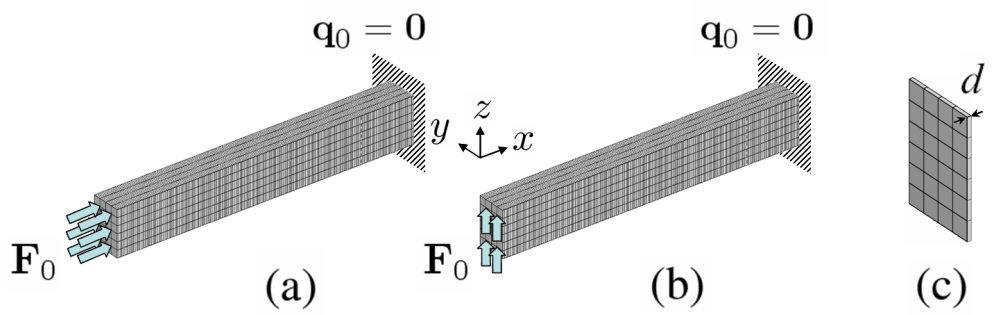


Figure 2: FE model of a clamped beam-like structure under longitudinal (a) or transverse (b) load; FE model of a typical substructure (c).

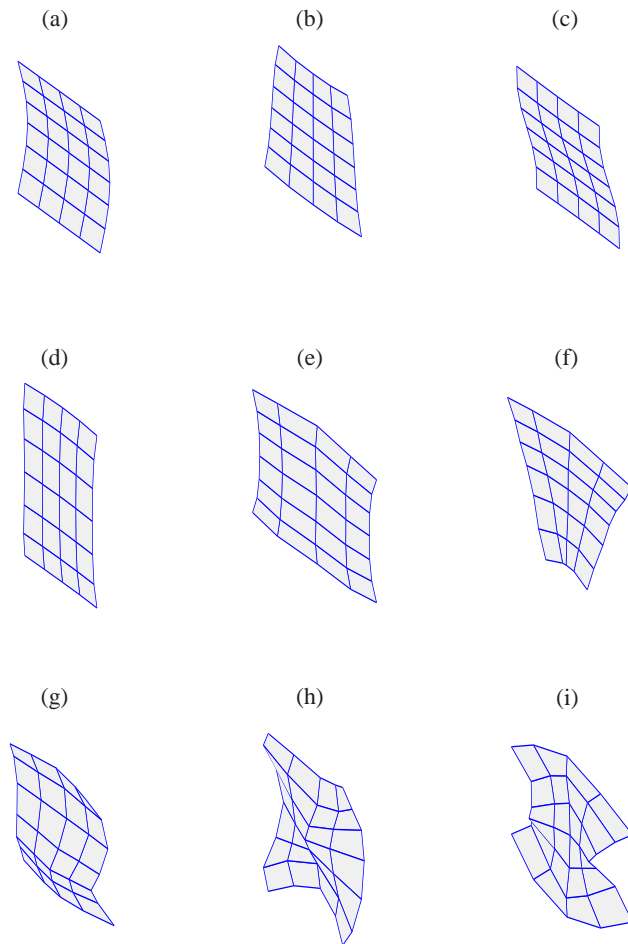


Figure 3: Spatial representation of several “cross-section” wave mode shapes for the beam-like structure depicted in Figure 2, at $7500Hz$: (a) longitudinal mode; (b) flexural mode; (c) shearing mode; (d-i) MF modes.

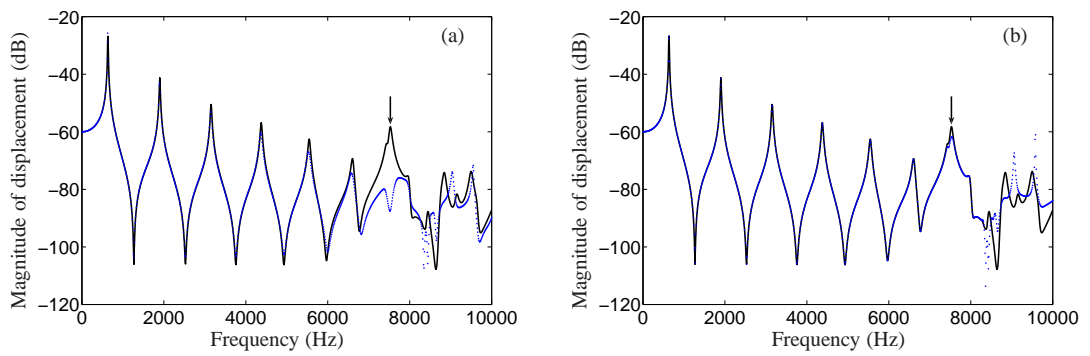


Figure 4: Frequency response of the clamped beam-like structure depicted in Figure 2, under longitudinal load: (—) solutions provided by FE; (· · ·) solutions provided by WFE with 10 modes (a) and 60 modes (b).

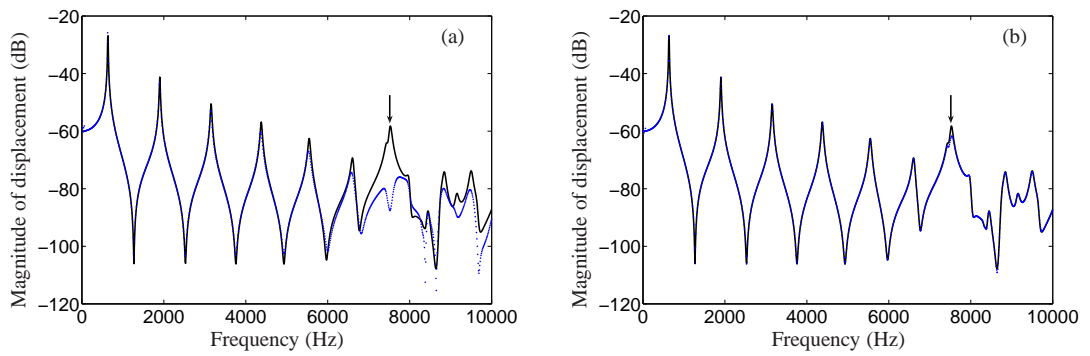


Figure 5: Frequency response of the clamped beam-like structure depicted in Figure 2, under longitudinal load: (—) solutions provided by FE; (· · ·) solutions provided by WFE — based on Eq. (13) — with 10 modes (a) and 60 modes (b).

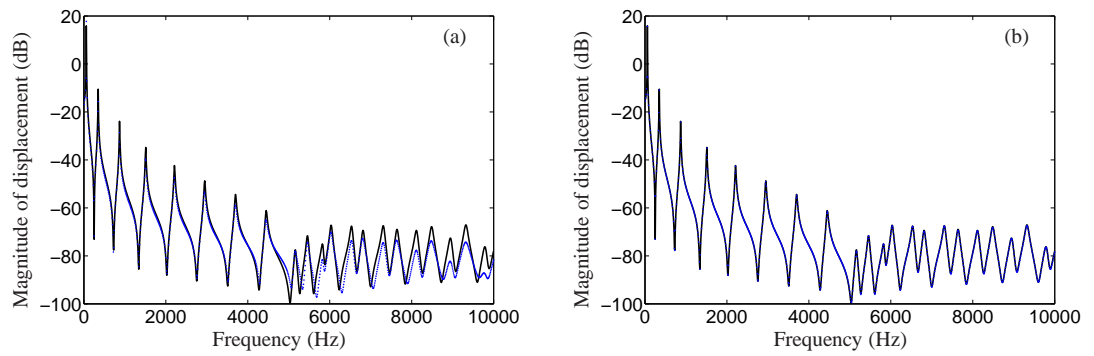


Figure 6: Frequency response of the clamped beam-like structure depicted in Figure 2, under transverse load: (—) solutions provided by FE; (\cdots) solutions provided by WFE — based on Eq. (13) — with 10 modes (a) and 40 modes (b).

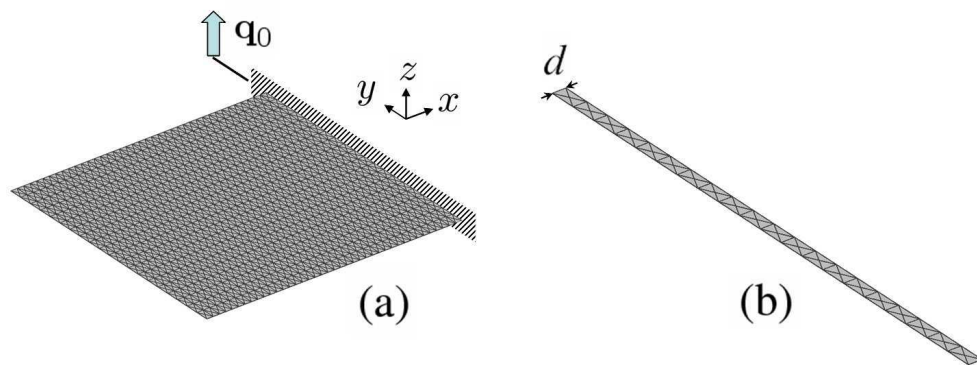


Figure 7: FE model of a Reissner-Mindlin plate with one edge clamped into a support with prescribed displacement (a); FE model of a typical substructure (b).

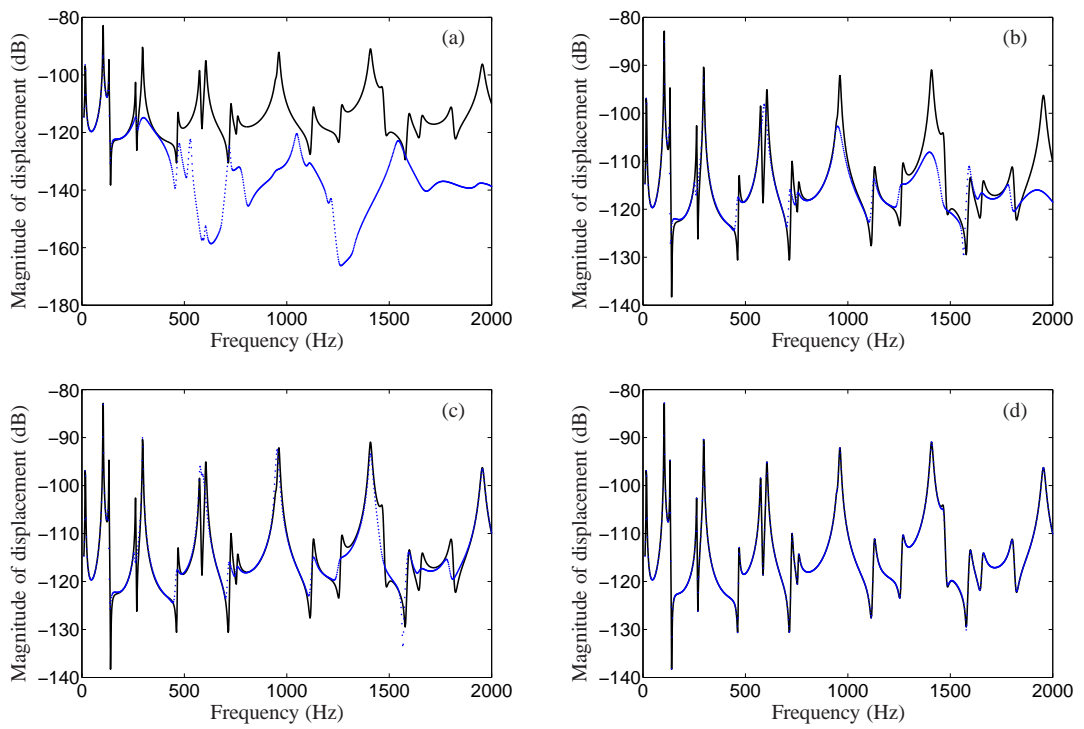


Figure 8: Frequency response of the Reissner-Mindlin plate depicted in Figure 7: (—) solutions provided by FE; ($\cdot\cdot\cdot$) solutions provided by WFE with 10 modes (a), 40 modes (b), 60 modes (c) and 80 modes (d).

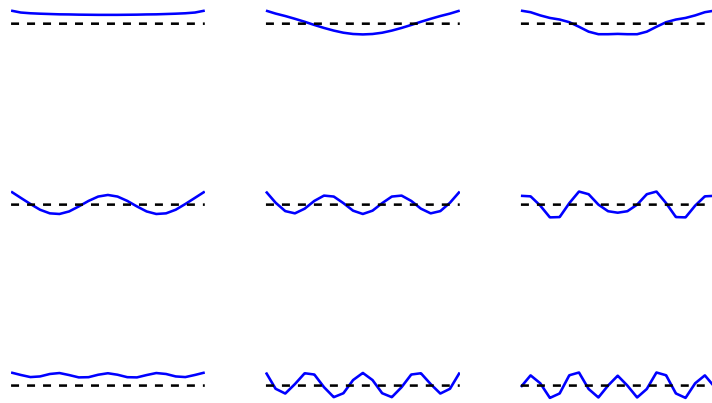


Figure 9: Spatial representation of several “cross-section” wave mode shapes for the Reissner-Mindlin plate depicted in Figure 7, at $1500Hz$: symmetric flexural LF and MF modes.

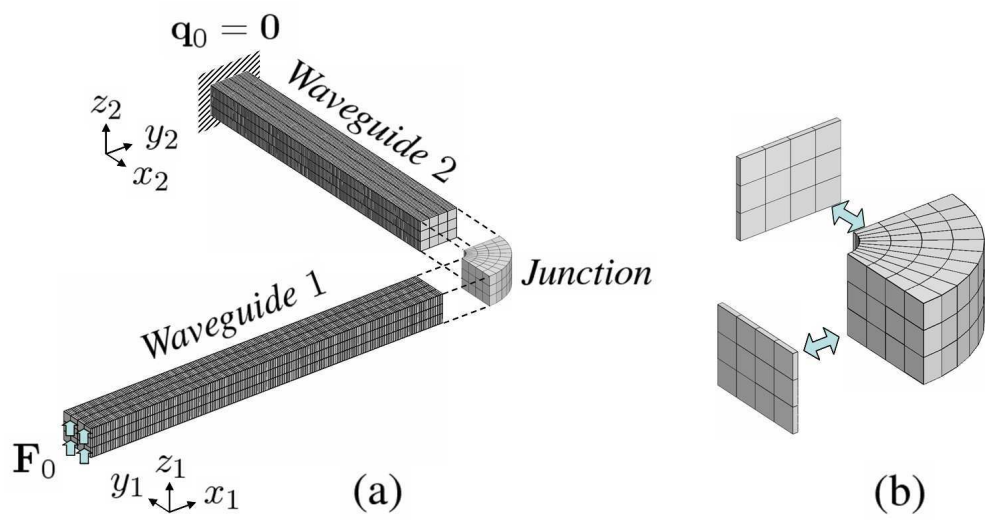


Figure 10: FE model of two waveguides coupled through an elastic junction (a); FE model of the underlying wave-based model, based on two coupled substructures (b).

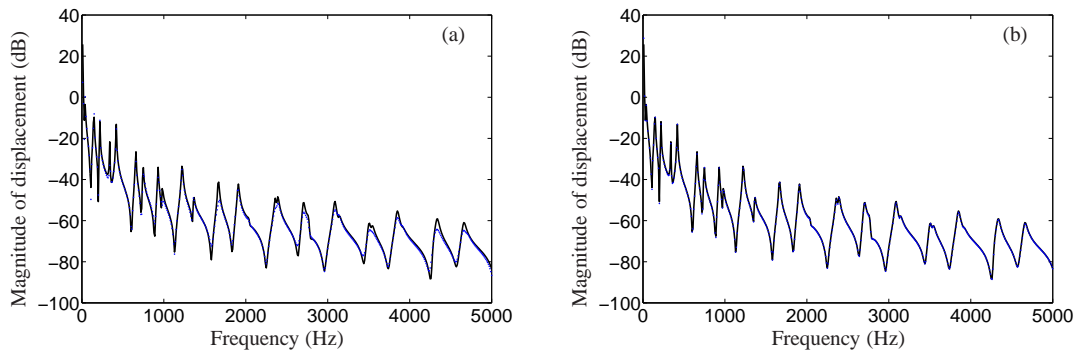


Figure 11: Frequency response of the coupled system depicted in Figure 10: (—) solutions provided by FE; (···) solutions provided by WFE with 10 modes (a) and 40 modes (b).

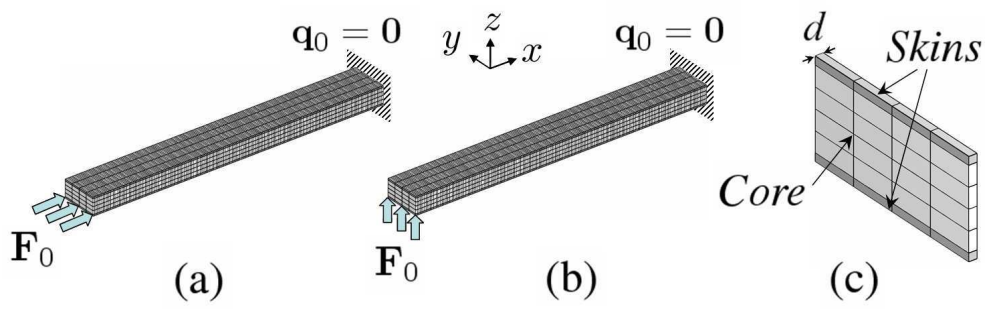


Figure 12: FE model of a sandwich beam under longitudinal (a) or transverse (b) load; FE model of a typical substructure (c).

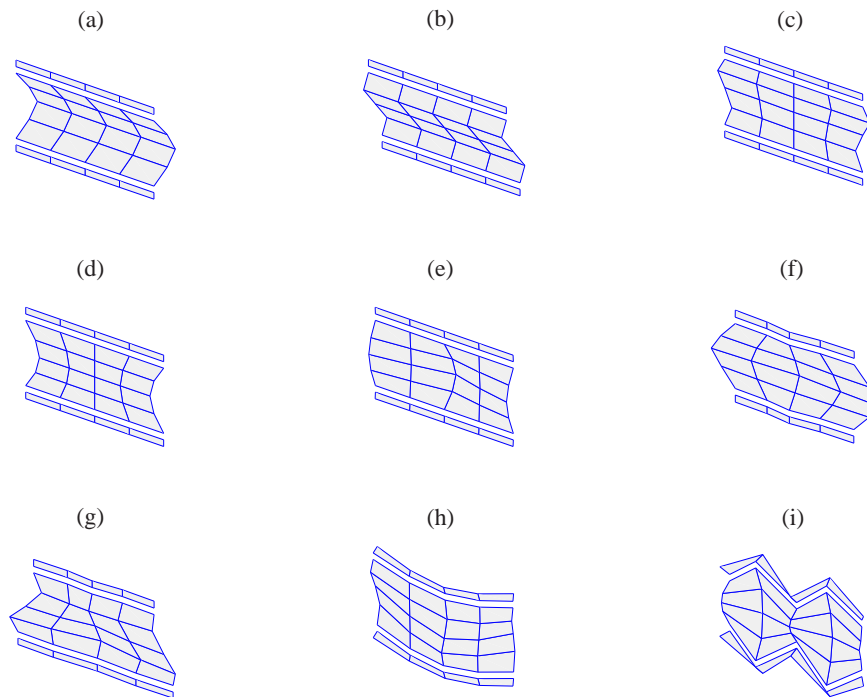


Figure 13: Spatial representation of several “cross-section” wave mode shapes for the sandwich structure depicted in Figure 12, at $1000Hz$: (a) longitudinal mode; (b) shearing mode; (c) flexural mode; (d-i) MF modes.

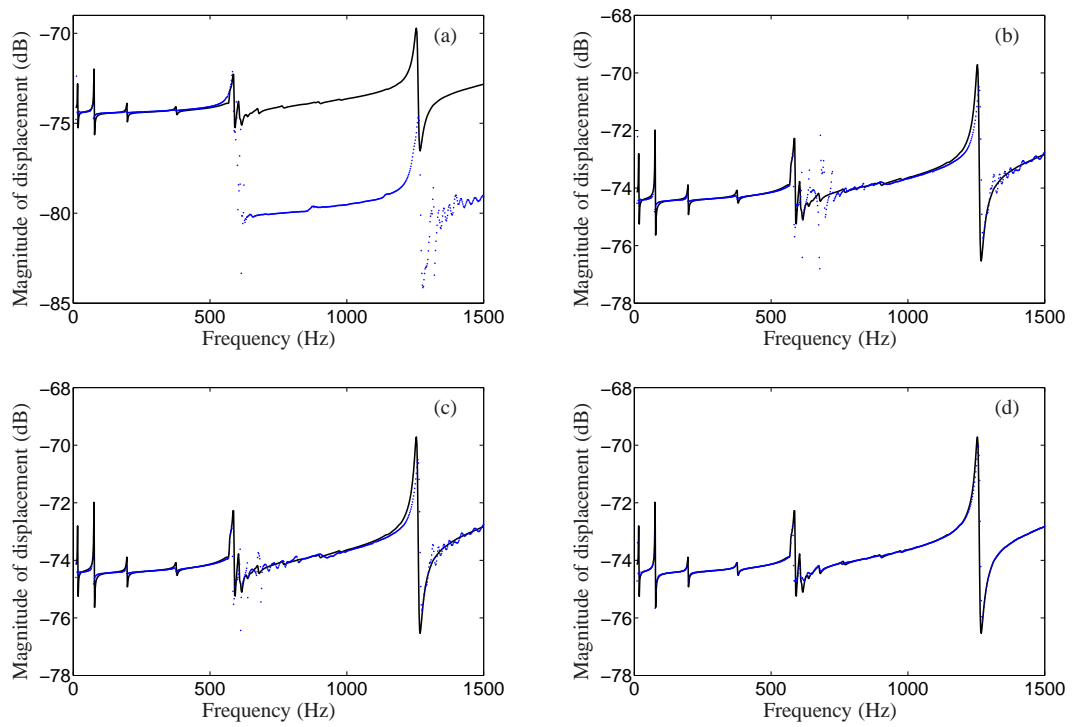


Figure 14: Frequency response of the sandwich structure depicted in Figure 12, under longitudinal load: (—) solutions provided by FE; (\cdots) solutions provided by WFE with 10 modes (a), 30 modes (b), 50 modes (c) and 70 modes (d).

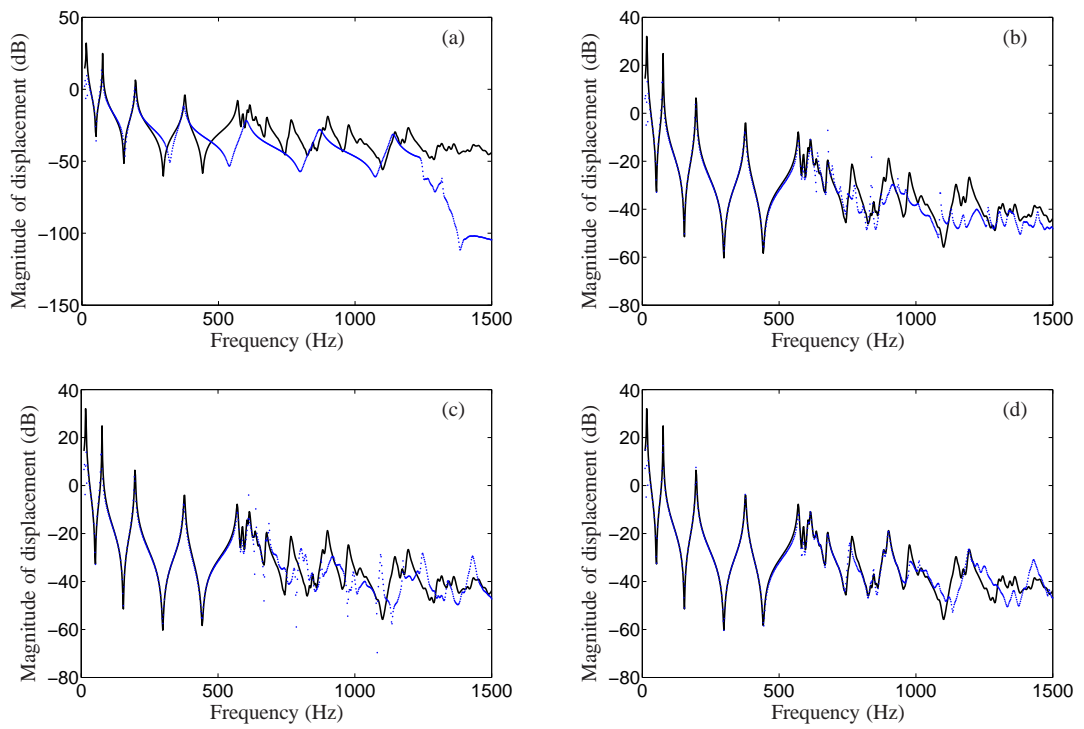


Figure 15: Frequency response of the sandwich structure depicted in Figure 12, under transverse load: (—) solutions provided by FE; (\cdots) solutions provided by WFE with 10 modes (a), 30 modes (b), 50 modes (c) and 70 modes (d).

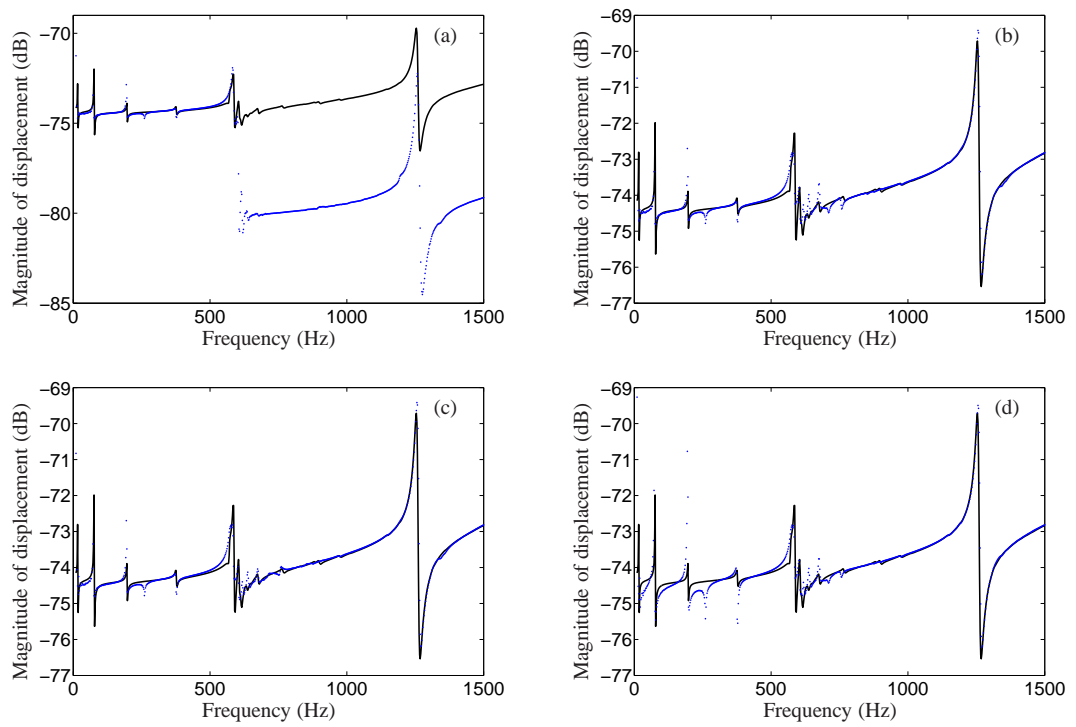


Figure 16: Frequency response of the sandwich structure depicted in Figure 12, under longitudinal load: (—) solutions provided by FE; (\cdots) solutions provided by regularized WFE with 10 modes (a), 30 modes (b), 50 modes (c) and 70 modes (d).

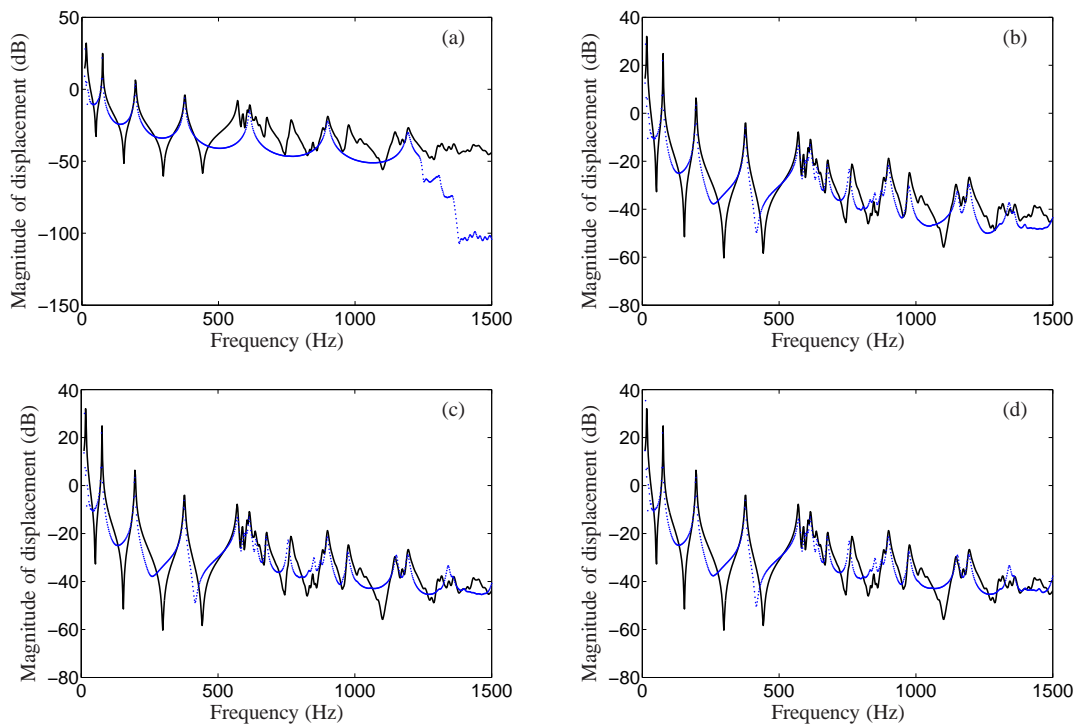


Figure 17: Frequency response of the sandwich structure depicted in Figure 12, under transverse load: (—) solutions provided by FE; (\cdots) solutions provided by regularized WFE with 10 modes (a), 30 modes (b), 50 modes (c) and 70 modes (d).

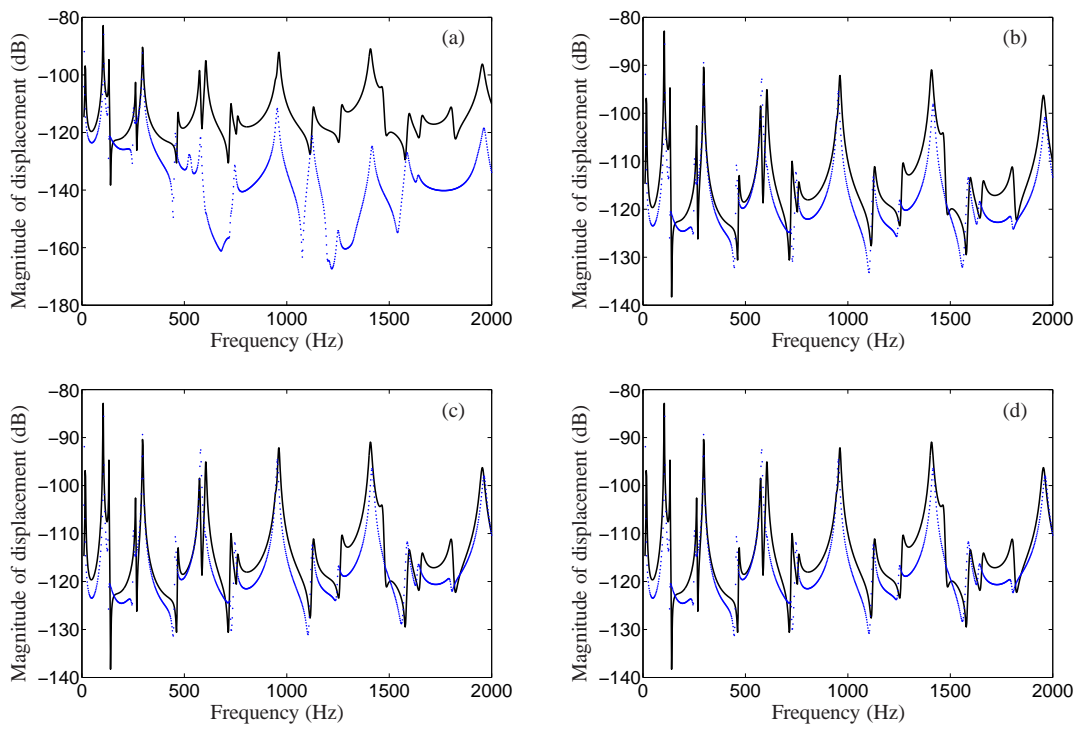


Figure 18: Frequency response of the Reissner-Mindlin plate depicted in Figure 7: (—) solutions provided by FE; (\cdots) solutions provided by regularized WFE with 10 modes (a), 40 modes (b), 60 modes (c) and 80 modes (d).